AI materials

Review

AI-Driven Optical Metamaterial Design: A Platform-Oriented Review

Guangyao Xu [1,2,†], Xiaolong Wei [1,2,†], Changhui Shen [1,2,†], Tongtong Song [1,2], Hongchen Chu [2,3], Jie Luo [2,4] and Yun Lai [1,2,*]

[1] National Laboratory of Solid State Microstructures, School of Physics, Collaborative Innovation Center of Advanced Microstructures, Nanjing University, Nanjing 210093, China
[2] Jiangsu Physical Science Research Center, Nanjing 210093, China
[3] School of Physics and Technology, Nanjing Normal University, Nanjing 210023, China
[4] School of Physical Science and Technology, Soochow University, Suzhou 215006, China
[*] Correspondence: laiyun@nju.edu.cn
[†] These authors contributed equally to this work.

Abstract

Artificial intelligence (AI), particularly deep learning (DL), is revolutionizing optical metamaterial design by overcoming the fundamental challenges of multidimensional parameter spaces, nonlinear structure–property relationships, and the intrinsic non-uniqueness of inverse problems. By learning complex mappings between geometric structures and electromagnetic responses, DL enables rapid forward prediction and on-demand inverse design without computationally intensive full-wave simulations. This review provides a comprehensive survey of AI-driven design methodologies across four key metamaterial platforms: localized resonant nanostructures, metasurfaces, periodic and guided-wave photonic structures, and complex scattering systems. For each platform, we systematically examine the neural network architectures employed, the specific design challenges addressed, and the representative achievements attained. These data-driven approaches not only significantly accelerate the discovery of high-performance structures but also offer new opportunities for extracting physical insights into light–matter interactions. We assess the critical challenges of data efficiency, model interpretability, and experimental feasibility, and outline emerging research directions that may address these barriers. This review aims to provide both a comprehensive summary of the current state of the art and forward-looking perspectives for this rapidly evolving interdisciplinary field.

Keywords: metamaterials; metasurfaces; scattering; deep learning; neural networks; inverse design

Academic Editor: Shuzhou Li

Received: 19 April 2026
Revised: 14 June 2026
Accepted: 29 June 2026
Published: 2 July 2026

1. Introduction

1.1. Research Significance and Challenges of Metamaterials

The history of human manipulation of light dates back thousands of years. From copper mirrors in ancient Egypt to modern optical fiber communications, each breakthrough has profoundly reshaped the course of civilization. However, the development of conventional optical devices has long been constrained by the electromagnetic properties of naturally occurring materials, limiting researchers to combinations and optimizations within a narrow range of refractive indices, dispersion, and anisotropy. This situation underwent a dramatic shift at the dawn of the 21st century. In 2000, Smith et al. [1] provided the first experimental verification of a composite medium exhibiting simultaneously negative permittivity and permeability, a concept theoretically predicted over three decades earlier [2]. In the same year, Pendry demonstrated that such materials could overcome the diffraction limit and achieve perfect lensing [3], and negative refraction was subsequently confirmed through direct observation [4]. These milestones proved that carefully engineered subwavelength artificial structures can produce electromagnetic responses unattainable in natural materials. These breakthroughs sparked widespread scientific interest in metamaterials and heralded the birth of an entirely new design paradigm [5]. Rather than passively accepting the material properties offered by nature, researchers could now actively construct artificial electromagnetic media tailored to specific requirements.

The revolutionary nature of metamaterials lies in shifting the determinant of optical properties from chemical composition to engineered geometric structure [6], thereby enabling on-demand control of light–matter interactions. On this basis, metamaterials have demonstrated remarkable capabilities over the past two decades, including electromagnetic cloaking enabled by transformation optics [7–9], super-resolution imaging beyond the diffraction limit [3,10], perfect absorbers [11], and topological photonics [12]. These achievements have not only broadened the scope of fundamental physics research but have also brought transformative solutions to emergent technological domains such as flat optics [13], bio-optics [14], and radiative cooling [15].

Nevertheless, the design and optimization of metamaterials face several fundamental challenges. From a computational standpoint, conventional design workflows rely heavily on electromagnetic simulations to evaluate candidate structures. The computational cost of a single full-wave simulation escalates sharply with structural complexity, and simulations of complex three-dimensional structures can require hours or even days [16]. Meanwhile, the dimensionality of the design space expands exponentially. When a metamaterial unit cell involves more than ten geometric parameters, multiple candidate materials, and broadband requirements, the number of potential design combinations can easily exceed one billion [17]. From a practical standpoint, although design experience and fundamental physical principles can be used to rule out many unreasonable candidates, increasing structural complexity often renders physical intuition ineffective. Researchers are then forced to conduct blind searches through vast candidate spaces, making the design process prohibitively difficult to complete.

The inverse design problem poses even greater challenges [18]. In the forward problem, given a set of structural parameters, the spectral response can be obtained through simulation. Inverse design, by contrast, requires deducing the geometric configuration that produces a desired response. Formally, let x denote the geometric and material parameters and y the corresponding electromagnetic response. The forward problem is a single-valued map that can be evaluated by full-wave simulation,

$$y = f(x), \qquad f : \mathcal{X} \to \mathcal{Y} \tag{1}$$

whereas inverse design seeks its reverse,

$$x = f^{-1}(y) \tag{2}$$

This inverse map is ill-posed: a target y may admit no exact solution, or multiple distinct structures may satisfy $f(x_1) \approx f(x_2) \approx y$ [19]. This non-uniqueness causes conventional optimization algorithms to become easily trapped in local optima and struggle to converge to the global optimum. These bottlenecks not only hinder the advancement of academic research but also impede the industrialization of metamaterial technologies, creating an urgent need for transformative methodological tools.

1.2. The Rise in AI and Its Role in Scientific Advancement

In recent years, the rapid development of AI, and machine learning (ML) in particular, has been driving a profound transformation of scientific research paradigms. Unlike traditional methods, the core idea of ML is to enable computers to autonomously learn the statistical relationships between inputs and outputs from data, identifying patterns, building models, and making predictions without explicit programming. Its greatest advantage lies in the ability to handle high-dimensional, highly complex problems that are difficult to address with conventional numerical and analytical approaches [20]. Deep learning (DL), a key evolution of ML, is built upon deep neural networks (DNNs) composed of multiple layers of nonlinear transformations [21]. The breakthrough of AlexNet in the 2012 ImageNet competition [22] demonstrated the ability of DNNs to extract hierarchical features from raw data. Since then, from AlphaGo defeating the world Go champion [23] to AlphaFold successfully predicting protein structures [24], and the emergence of architectures such as generative adversarial networks (GANs) [25] and Transformers [26], AI has continuously pushed the performance frontier in image recognition, natural language processing, biomedical diagnostics, and numerous other fields.

In materials science, AI has given rise to three core application paradigms [27]. First, forward prediction employs neural networks as surrogates for time-consuming physical simulations, achieving orders-of-magnitude acceleration. Second, inverse design generates material structures that satisfy target performance specifications in reverse, overcoming the limitations of traditional trial-and-error approaches. Third, accelerated optimization leverages Bayesian strategies to identify optimal materials with minimal experimentation. The first two paradigms are realized by training a neural network f_θ to approximate the forward or inverse map, with its parameters θ optimized by minimizing a loss over N samples. The most common objectives are the mean squared error (MSE),

$$\mathcal{L}_{MSE} = \frac{1}{N}\sum_{i=1}^{N} \|f_\theta(x_i) - y_i\|^2 \tag{3}$$

and the mean absolute error (MAE),

$$\mathcal{L}_{MAE} = \frac{1}{N}\sum_{i=1}^{N} |f_\theta(x_i) - y_i| \tag{4}$$

Physics-informed training augments the data loss with a penalty enforcing the governing equations,

$$\mathcal{L} = \mathcal{L}_{\text{data}} + \lambda\mathcal{L}_{\text{physics}} \tag{5}$$

where $\mathcal{L}_{\text{physics}}$ is the residual of the relevant physical constraint such as Maxwell's equations and λ balances data fidelity against physical consistency.

1.3. Convergence and Mutual Empowerment of Metamaterials and AI

The design requirements of metamaterials and the capabilities of DL form a natural synergy. The "structure determines function" nature of metamaterials means that their design is essentially a search for optimal configurations in a high-dimensional geometric space that satisfy target responses. This requires design methods capable of simultaneously optimizing multiple coupled objectives. Neural networks excel at precisely this type of high-dimensional, nonlinear, multi-objective optimization problem, making the combination of the two a natural and inevitable development [28].

Before the introduction of DL, metamaterial design relied primarily on two categories of methods. The first is topology optimization [19,29], which iteratively adjusts the material distribution within a pixelated design domain to maximize an objective function. This approach has been successfully applied to the design of photonic crystal waveguides and mode converters, among other devices. While mathematically rigorous, it is computationally expensive and sensitive to initial conditions. The second category comprises heuristic algorithms, including genetic algorithms [30] and particle swarm optimization [31], which search for optimal solutions by mimicking natural evolution or swarm behavior. However, these methods suffer from slow convergence and difficulty in handling high-dimensional problems.

The turning point came around 2018, when DL began to be systematically applied to metamaterial design. Peurifoy et al. first demonstrated that trained neural networks could approximate the light scattering properties of multilayer nanoparticles, achieving prediction speeds several orders of magnitude faster than conventional simulations, and realized inverse design through backpropagation [32]. In the same year, Liu et al. proposed the tandem network architecture to address the non-uniqueness problem in inverse design [33], and Ma et al. applied DL to the design of three-dimensional chiral metamaterials [34]. Since then, multiple DL paradigms, including GANs [35], variational autoencoders (VAEs) [36], and reinforcement learning (RL) [37], have been successively introduced, progressively shifting metamaterial design from human-driven simulation iteration toward data-driven intelligent optimization.

It is worth noting that the relationship between metamaterials and AI is one of mutual empowerment. Beyond AI providing powerful computational tools for metamaterial design, metamaterials are equally opening new pathways for the hardware implementation of AI. Traditional electronic computing architectures face the dual challenges of Moore's law scaling limits and the von Neumann bottleneck, while photonic systems, with their inherent parallelism, high bandwidth, and low power consumption, are emerging as important platforms for the physical realization of neural networks [38]. This bidirectional relationship forms a positive feedback loop, in which AI drives metamaterials toward greater complexity and higher performance, while advanced metamaterials in turn provide more powerful physical platforms for AI implementation.

1.4. Scope and Classification of This Review

Several recent reviews have surveyed the use of AI in metamaterial design [16,28,38]. Most are organized around neural network architectures, with photonic platforms appearing as case studies of how each network is deployed. A broader cross-domain review covers AI applications spanning optical, acoustic, healthcare, and power-system metamaterials [39]. Both framings serve their respective readers but offer limited guidance for photonics researchers who already work within a specific physical domain and seek the AI tools that match their design problem. This review addresses this gap with a platform-oriented organization, so that researchers can quickly locate the AI methods relevant to their own field. We first summarize the principal DL paradigms used in the field, and then introduce the four metamaterial platforms that form the structural backbone of this review.

From the perspective of network architecture, current research encompasses a wide range of DL paradigms. Fully connected neural networks (FCNNs) represent the most fundamental architecture and are suitable for modeling low-dimensional parameterized structures [32]. Convolutional neural networks (CNNs) excel at processing image-based designs with spatial structure and can automatically extract local features [40]. To address the non-uniqueness problem in inverse design, tandem networks cascade a pre-trained forward network with an inverse network, mitigating the difficulties of one-to-many mapping through forward constraints [41]. GANs generate diverse structures satisfying target responses through adversarial training [42]. VAEs encode the design space into a continuous low-dimensional latent space, facilitating interpolative search and uncertainty quantification [43]. Furthermore, RL optimizes design strategies through agent-environment interaction [44], and neural adjoint methods combine gradient-based optimization to achieve efficient inverse solving [45]. These paradigms emerged and matured over little more than a decade. Figure 1 places the principal milestones of metamaterials design in chronological order, from the enabling deep learning advances to the recent foundation models and autonomous agents.

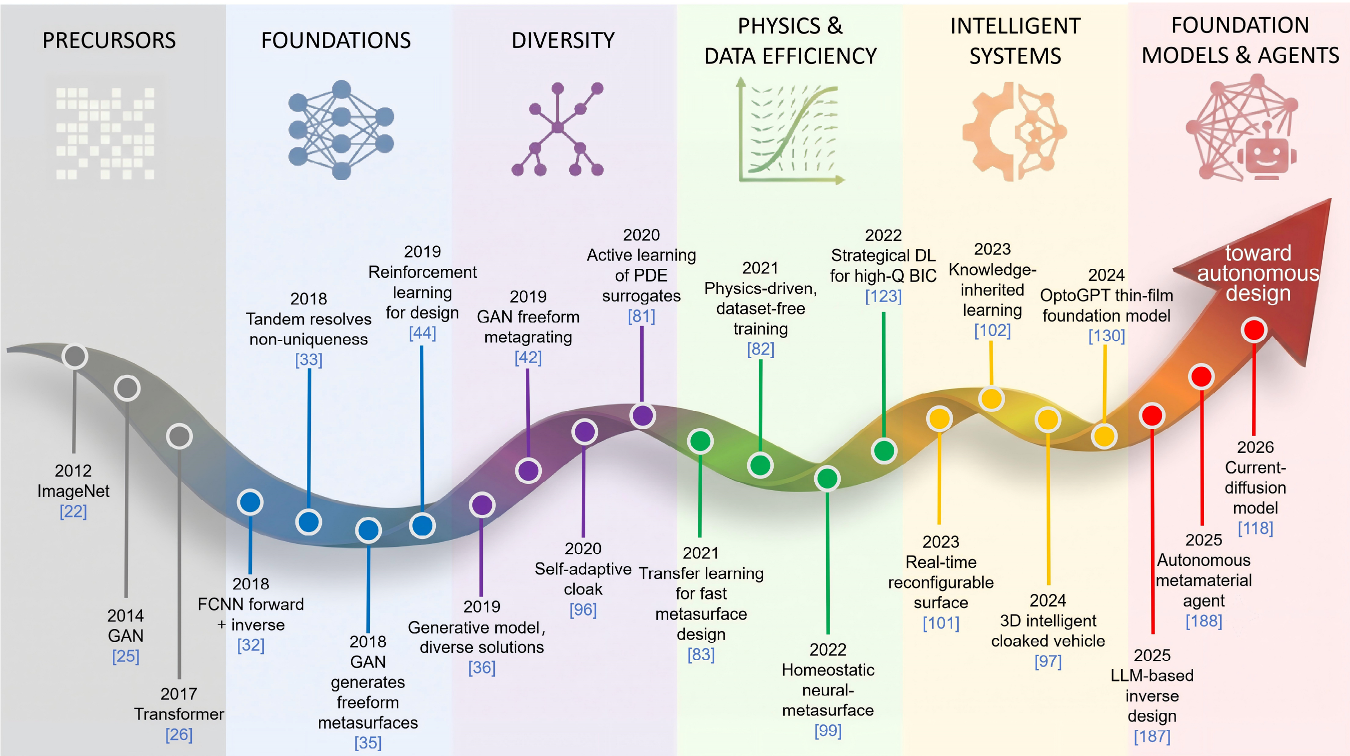

Figure 1. Timeline of representative milestones in AI-driven optical metamaterial design. The works are placed in chronological order and grouped into six eras, drawn as colored bands that shift from cool to warm tones to mark the field's progression.

From the perspective of the underlying electromagnetic platform, this review classifies the research subjects into four major categories, each characterized by distinct physical mechanisms, design space properties, and AI modeling requirements. *Localized resonant nanostructures*, including plasmonic and all-dielectric Mie resonators, are characterized by subwavelength electromagnetic energy confinement and low-dimensional parametric design spaces [46,47]. Their relatively simple structure-response relationships make them ideal testbeds for establishing foundational deep learning methodologies.

Metasurfaces manipulate the amplitude, phase, and polarization of light through two-dimensional arrays of subwavelength unit cells, enabling functionalities such as lensing [48], holography [49], beam shaping [50], perfect absorption [11], and polarization conversion [51]. Their design space grows exponentially with the number of unit cells, making metasurfaces the most active and challenging platform for AI-assisted design.

Periodic and guided-wave photonic structures, primarily photonic crystals (PCs) [52,53] and their derived waveguide and cavity devices, exhibit optical properties governed by photonic bandgaps and Bloch modes arising from periodic dielectric modulation [54]. The periodicity constraint partially limits the design degrees of freedom, but the eigenvalue nature of bandgap and Q-factor calculations introduces distinct computational challenges for AI methods [55–57].

Complex scattering systems, encompassing disordered scattering media, biological tissues, and multimode fibers, differ fundamentally from the above three deterministic platforms in that light propagation involves the coherent superposition of numerous random scattering events [58,59]. Their input-output relationships are described by high-dimensional transmission matrices [60], and DL has demonstrated unique advantages in learning the statistical properties of scattering for applications in imaging [61,62], wavefront shaping [63,64], and fiber-optic transmission [65,66].

1.5. Organization of This Review

Sections 2–5 discuss the four metamaterial platform categories in sequence: localized resonant nanostructures, metasurfaces, periodic and guided-wave photonic structures, and complex scattering systems. Each chapter provides the relevant physical background in detail and then analyzes the specific implementation strategies and representative applications of forward modeling and inverse design in the context of the corresponding platform. Section 6 evaluates the current challenges from three perspectives, namely data efficiency, model interpretability, and experimental feasibility, and provides an outlook on future directions for the field.

2. Localized Resonant Nanostructures

Plasmonic nanostructures exploit localized surface plasmon resonances (LSPRs) arising from collective electron oscillations at metal-dielectric interfaces, enabling extreme field enhancement and subwavelength light confinement [46]. All-dielectric nanostructures based on high-refractive-index materials, on the other hand, support Mie-type electric and magnetic dipolar resonances without ohmic losses [47]. Both systems share a common design characteristic: their optical responses are governed by a finite set of geometric parameters such as dimensions, shapes, and material compositions, forming a low-dimensional continuous parameter space amenable to neural network regression [67]. This low dimensionality plays a crucial role in determining appropriate neural network architectures. Because localized resonant nanostructures involve relatively few design parameters, even conventional computational methods remain feasible for individual simulations, but the speed advantage of neural network surrogates becomes decisive when exhaustive design space exploration is required. This characteristic makes localized resonant nanostructures ideal platforms for establishing and validating foundational deep learning methodologies before extending them to higher-dimensional systems.

2.1. Forward Modeling

The pioneering work by Peurifoy et al. established the foundation for neural network-based forward modeling of resonant nanostructures as shown in Figure 2a [32]. Using a four-layer FCNN, they predicted the scattering spectra of multilayer core–shell nanospheres from eight geometric parameters, achieving prediction speeds orders of magnitude faster than numerical calculations. Importantly, this work provided clear evidence that the network learns the underlying physics of the system rather than performing simple data interpolation. This dramatic acceleration enabled exhaustive design space exploration previously infeasible with conventional simulations.

Subsequent work expanded the scope of forward modeling along two directions: handling increasingly complex geometries and incorporating physical constraints to improve accuracy. Malkiel et al. introduced a bidirectional FCNN architecture for plasmonic nanostructure design and characterization as shown in Figure 2b [68]. The network jointly trains an inverse path that predicts geometry from far-field spectra and a forward path that predicts spectra from geometry, with this bidirectional training achieving significantly higher accuracy than separately trained networks. Applied to parameterized H-shaped gold nanostructures with variable edge lengths and angles, this approach was experimentally validated by retrieving subwavelength geometric dimensions from measured far-field transmission spectra alone. He et al. further extended the scope of DNN-based forward modeling from far-field spectra to two-dimensional near-field electromagnetic enhancement distributions around plasmonic nanoparticles [69], achieving predictions approximately six orders of magnitude faster than conventional numerical simulations through screening and resampling methods that greatly reduce the amount of electromagnetic data. These two advances are complementary. The former demonstrates that bidirectional network architectures enable simultaneous forward prediction and inverse characterization with experimental validation, while the latter extends neural network surrogates beyond spectral prediction to spatially resolved near-field distributions critical for applications such as surface-enhanced Raman spectroscopy.

Wiecha et al. demonstrated that neural networks can enable optical retrieval of digital information encoded in the geometries of subwavelength silicon nanostructures, achieving quasi-error-free readout of sequences up to 9 bits and pushing the limits of optical information storage density [70]. This application illustrates that trained neural network models can serve purposes well beyond conventional design tasks. Wiecha and Muskens subsequently developed a generalized predictor based on a three-dimensional fully convolutional neural network capable of handling arbitrary 3D nanostructures, demonstrating accurate prediction of both near-field distributions and far-field scattering spectra for plasmonic and dielectric systems without requiring specific training for individual physical effects as shown in Figure 2c [71].

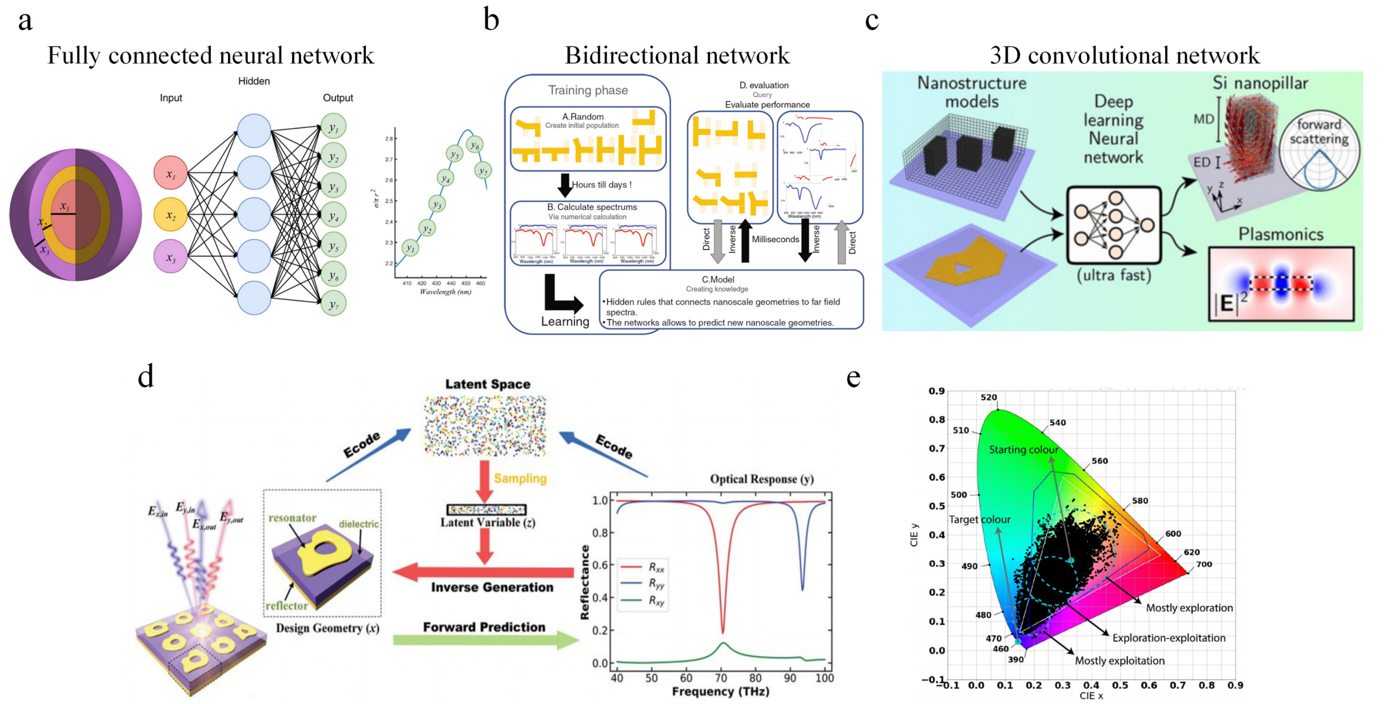

Figure 2. (**a**) Schematic of multilayer core–shell nanosphere (**left**), fully connected neural network architecture for scattering spectrum prediction (**middle**), and comparison between the network output and the simulated scattering spectrum (**right**) (reproduced from [32]). (**b**) Bidirectional design workflow for plasmonic H-shaped nanostructures: numerical generation of random geometries and spectra (**left**), network learning of hidden geometry–spectrum rules (**middle**), and millisecond bidirectional evaluation for forward prediction and inverse retrieval (**right**) (reproduced from [68]). (**c**) Unified deep learning framework for arbitrary 3D nanostructures (**left**), forward prediction of scattering response and electric/magnetic multipole decomposition for a silicon nanopillar (**top right**), and predicted near-field intensity distribution for a plasmonic nanostructure (**bottom right**) (reproduced from [71]). (**d**) Semi-supervised deep generative model for chiral metamaterial inverse

design: schematic of meta-atom with resonator, dielectric spacer, and reflector under orthogonal polarization (**left**), encoder–decoder mapping geometry and optical response to a shared latent space (**middle**), and reflectance spectra of a generated structure (**right**) (reproduced from [36]). (**e**) CIE chromaticity diagram showing deep Q-learning exploration process for structural color design of silicon nanostructures, with trajectory from start to target color under decreasing exploration ratios (reproduced from [44]).

2.2. Inverse Design

The inverse design of localized resonant nanostructures confronts the fundamental challenge of non-uniqueness: multiple geometries may produce similar optical responses. This one-to-many mapping makes inverse problems inherently ill-posed, as neural networks face conflicting gradients during training when different geometric configurations yield identical spectral targets [67]. A variety of strategies have been developed to address this challenge, broadly falling into deterministic architectures, generative models, and optimization-guided approaches.

Deterministic architectures: Liu et al. proposed the tandem architecture, in which a pre-trained forward network is concatenated with an inverse network during training [33]. The forward network is first trained independently and then fixed, forcing the inverse network to converge toward physically valid solutions. The loss function, computed in the spectral domain rather than the structural domain, allows the network to discover any valid solution without penalization for selecting structures that differ from the training data. This architecture has become foundational for nanophotonic inverse design. Wu et al. systematically compared iterative and tandem networks for plasmonic nanoantenna design, providing practical guidelines for architecture selection based on design complexity and target specifications [72]. Gao et al. took a different approach by training forward and inverse networks jointly within a bidirectional architecture for silicon nanostructure design [41]. Applied to structural color generation, this approach achieved high-fidelity color reproduction across the visible spectrum, demonstrating the practical utility of simultaneously learning both mapping directions. So et al. further extended the scope of deterministic inverse design by simultaneously optimizing material composition and geometric parameters for core–shell nanoparticles [73]. Their neural network predicts both dimensional parameters and material types for dipole resonance engineering, demonstrating that the design degrees of freedom accessible to DNN-based inverse approaches can encompass discrete material choices alongside continuous geometric variables. Guo et al. extended deep learning-assisted scattering design beyond the subwavelength regime to electromagnetically large nonmagnetic cylinders [74]. By developing a hybrid neural network that combines the forward network of one polarization with the inverse network of another, they achieved electromagnetic duality symmetry beyond the dipolar approximation, constructing dual-paired cylinders with matched angular scattering patterns for cross polarizations. Adibnia et al. extended DNN-based forward modeling and inverse design to all-optical nonlinear plasmonic ring resonator switches, demonstrating computational efficiency surpassing traditional FDTD-based approaches [75,76].

Generative models: While deterministic architectures output a single solution for each target, generative models aim to capture the full probability distribution of valid designs, naturally accommodating the one-to-many mapping inherent in inverse problems. Rahman et al. employed conditional variational autoencoders (cVAEs) for core–shell nanoparticle inverse design, demonstrating that cVAEs achieve lower mean absolute error and higher robustness compared to tandem networks while generating multiple valid solutions for identical target spectra [77]. Ma et al. proposed a probabilistic representation framework based on deep generative models with a semi-supervised learning strategy for nanostructure inverse design, enabling enhanced diversity and accuracy in generated solutions as shown in Figure 2d [36]. Together, these works illustrate that generative approaches not only resolve the non-uniqueness problem but also provide designers with a diverse set of physically valid candidates, offering greater flexibility in balancing multiple design constraints.

Optimization-guided and reinforcement learning approaches: Hybrid strategies combining neural network surrogates with optimization algorithms offer another route to address the one-to-many mapping challenge. By connecting a trained forward neural network with heuristic algorithms such as evolutionary algorithms, closed-loop systems can rapidly generate candidate nanostructures after iterations, with the neural network serving as a high-speed surrogate for electromagnetic simulators [78]. In a conceptually different direction, Sajedian et al. pioneered the application of deep Q-learning to optimize the morphology of silicon nanostructures for structural color generation [44]. The RL agent explores the parameter space guided by the matching level between simulated reflection spectra and target color standards, finding optimal configurations within 9000 steps from millions of possible states as shown in Figure 2e. This approach achieved purer colors compared to previously reported results, demonstrating that RL offers a viable alternative to supervised learning paradigms when the design objective can be naturally formulated as a reward function.

Localized resonant nanostructures, with their low-dimensional parameter spaces and well-characterized physical responses, have served as the proving ground for the major deep learning strategies now applied across nanophotonics. The fundamental challenge of non-uniqueness has driven significant methodological innovation, progressing from Peurifoy et al.'s foundational demonstration that neural networks capture underlying physics rather than memorizing data [32], through Liu et al.'s tandem architecture that resolves training conflicts from non-unique instances [33], to generative models that produce diverse solution sets by learning probability distributions [36]. These methodological foundations extend directly to the more complex and higher-dimensional systems discussed in subsequent chapters, where additional challenges arising from exponentially larger design spaces and eigenvalue-based physics will demand further architectural innovations.

3. Metasurfaces

Metasurfaces [79] are two-dimensional arrays composed of subwavelength artificial structures (meta-atoms). They enable the precise manipulation of the phase [80–84], amplitude [85–90], and polarization state [91–93] of electromagnetic waves. This capability has led to a range of functional categories, from single-dimension control to multifunctional integration [93–95] and reconfigurable dynamic control [96–106], thereby laying the physical foundation for applications such as metalenses [80], multifunctional holography [94], intelligent cloaking [96–98], smart communications [99–103], and intelligent sensing [104–106].

However, the design and simulation of metasurfaces face numerous challenges. A typical functional metasurface can contain hundreds to tens of thousands of unit cells, each with multiple continuous or discrete geometric degrees of freedom. When considering free-form topologies, the design parameter space expands further to the pixel level, making traditional parameter sweeping and empirical trial-and-error methods incapable of traversing all feasible solutions within a reasonable timeframe. Furthermore, in high numerical aperture, densely packed metasurface architectures, the failure of the local phase approximation necessitates the consideration of near-field coupling [107]. More critically, the inherent non-uniqueness problem in inverse design of metasurfaces leads to nonconvergence in traditional inverse mapping [33]. Reconfigurable metasurfaces introduce the additional dimension of dynamic environmental adaptation, requiring the completion of sensing-decision-action closed-loop control within millisecond time scales [96]. These multi-level challenges, ranging from the unit cell to the system and from static to dynamic operation, render traditional optimization methods based on parameter sweeping and trial-and-error inadequate.

Since 2018, deep learning methods have been systematically introduced into the field of metasurfaces and have rapidly developed into core tools for addressing these challenges. Peurifoy et al. [32] used multilayer perceptrons to accelerate full-wave simulations by a factor of ten thousand, Liu et al. [33] proposed tandem networks to resolve the inverse non-uniqueness problem, and Liu et al. [35] employed GANs for freeform shape generation, collectively laying the foundation for data-driven metasurface design. For a comprehensive overview of machine learning, physics-informed neural networks, and topology optimization methods applied to metasurface design, the reader is referred to a recent review [108]. This chapter reviews research progress along the two major directions of forward modeling and inverse design, organized according to the functional classification of metasurfaces. For inverse design, we further distinguish between static metasurfaces and reconfigurable metasurfaces, as the latter involve real-time closed-loop control that introduces distinct methodological requirements.

3.1. Forward Modeling

Phase modulating: In the forward modeling of phase-modulating metasurfaces, the 180° phase jumps induced by electromagnetic resonances have long posed a fundamental challenge to accurate neural network learning. To address this, An et al. proposed a Predictive Neural Network (PNN) based on a Neural Tensor Network (NTN) for the efficient modeling of all-dielectric meta-atoms as shown in Figure 3a [40]. By introducing a bilinear tensor layer, the network directly captures the multiplicative physical relationships among design parameters. The key innovation of this work is shifting the prediction target from phase and amplitude to the real and imaginary parts of the complex transmission coefficient, thereby circumventing the phase discontinuity problem. This representation strategy has since become a widely adopted practice in metasurface forward modeling.

An et al. subsequently extended this framework to a CNN-based PNN for modeling three-dimensional meta-atoms with higher degrees of freedom [80]. The network adopts a dual-input architecture, processing a one-dimensional property vector (refractive index, thickness, lattice size) and two-dimensional freeform patterns through separate branches before feature fusion. This model predicts the spectral responses of complex geometric structures within milliseconds and maintains prediction accuracy for unseen features such as ring-shaped patterns, reducing computation time for tasks such as phase coverage evaluation and metalens optimization from hours to seconds.

While the above approaches focus on network architecture design, Pestourie et al. [81] tackled the problem from the perspective of training data efficiency. They introduced an active learning framework employing an ensemble neural network that simultaneously outputs predictions of the complex transmission coefficient along with their uncertainty estimates. By iteratively selecting samples with the highest uncertainty for full-wave simulation and incorporation into the training set, this approach reduces the required training data by more than an order of magnitude while maintaining two-orders-of-magnitude speedup over direct PDE solvers. This data-efficient strategy is complementary to the architectural innovations described above and is particularly valuable for large-scale metasurface optimization where simulation costs are prohibitive.

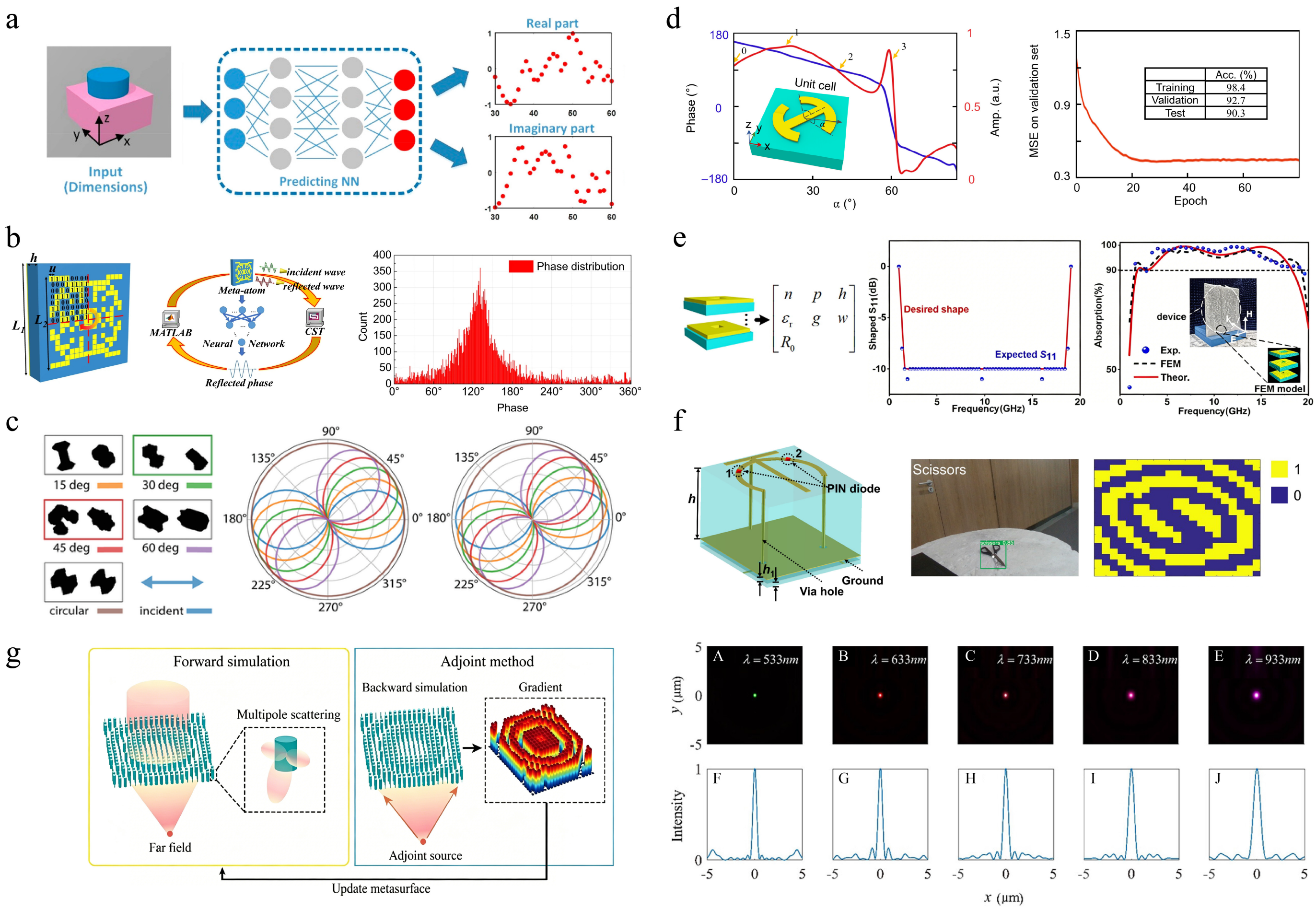

Figure 3. (**a**) Input structure of the PNN (**left**), architecture of the PNN (**middle**), and discrete output samples of the real and imaginary parts predicted by the PNN (**right**) (reproduced from [40]). (**b**) Discretization and coding of the meta-atom pattern (**left**), schematic of the data collection process based on MATLAB-CST co-simulation (**middle**), histogram of the phase distribution of the dataset generated by the neural network (**right**) (reproduced from [83]). (**c**) Unit cells of designed diatomic metamolecules (**left**), simulated polarization states of transmitted light from the metamolecules with a neural network simulator (**middle**) and FEM full-wave simulation (**right**) (reproduced from [92]). (**d**) Reflected response of the neuro-metasurface (**left**). Phase (blue) and amplitude (red) vs. rotation angle α at 13.4 GHz. Training accuracy over epochs (**right**) (reproduced from [99]). (**e**) The n-layer meta-atom is defined by seven input parameters (**left**), expected "U"-shaped S_{11} (**middle**), realized S_{11} of the absorber, showing a wideband of high absorption (**right**) (reproduced from [109]). (**f**) Schematic of the designed meta-atom (**left**), one of the target examples in experiments (**middle**), retrieved coding matrix by the modified GS algorithm (**right**) (reproduced from [110]). (**g**) The inverse-design framework based on multipole decomposition and adjoint optimization (**left**), focal electric field intensity distribution at five design wavelengths (**right**) (reproduced from [111]).

Amplitude-modulating: Forward modeling of amplitude-modulating metasurfaces has evolved along two parallel directions, namely expanding geometric input representations and improving spectral output predictions. In the first direction, Inampudi and Mosallaei [85] demonstrated a three-layer feedforward neural network that maps geometric parameters of metagrating units to diffraction efficiencies, with training data generated via rigorous coupled-wave analysis (RCWA). Sajedian et al. [86] further removed the constraint of parametric geometry by proposing a hybrid CNN-RNN model that directly predicts absorption spectra from two-dimensional images of plasmonic structures. In this approach, three-dimensional structures with fixed thickness and material are first projected into 2D images, the CNN extracts spatial features, and the subsequent RNN learns the mapping between these features and the absorption spectrum sequence. This image-based approach demonstrated that CNNs can effectively handle non-parametric, high-degree-of-freedom geometric inputs, significantly expanding the accessible design space.

In the second direction, treating spectral data as sequential signals has emerged as an effective strategy for improving prediction accuracy. Pillai et al. introduced long short-term memory (LSTM) networks for forward modeling of metamaterial absorption spectra in the terahertz regime [87]. By exploiting the gating mechanism of LSTMs to capture spectral correlations, this approach achieved significantly better prediction accuracy than feedforward networks using multilayer perceptrons alone, highlighting the advantage of sequential modeling for spectral data.

Polarization-modulating: Colorimetric optical detection based on structural colors provides a novel paradigm for compact polarization measurement. Yang et al. proposed a quantitative colorimetric polarization-angle detection method based on asymmetric all-dielectric metasurfaces [91]. By independently tuning the periods and diameters of the nanopillars along the x and y axes, the metasurface enables arbitrary dual-color switching under orthogonal polarization states. A Polarization Detection Network (PDN) constructed on the ResNet-34 architecture learns the mapping between color variations and the incident polarization angle, achieving high-precision detection within approximately one second. Compared to traditional methods relying on birefringent or dichroic elements paired with power meters, this approach offers significant improvements in both system integration and detection efficiency.

Coupling effects: Conventional metasurface design typically assumes periodic boundary conditions, neglecting the near-field coupling caused by aperiodic arrangements, which leads to degraded device performance. Two complementary approaches have been developed to address this limitation. An et al. proposed a CNN-based forward prediction model that takes the geometric dimensions of a target meta-atom and its neighboring units as input, enabling the rapid prediction of localized phase and amplitude responses that account for mutual coupling [107]. The effectiveness of this approach was validated through the optimized design of a beam deflector and a metalens, both showing significantly enhanced efficiency compared to designs that neglect coupling.

Wu et al. [112] approached the coupling problem from a fundamentally different perspective by introducing graph neural networks (GNNs). In this framework, metasurface units are modeled as nodes in a graph data structure, and the coupling relationships between units are quantified as edge features. Graph convolutional layers perform message passing and feature aggregation, thereby embedding coupling effects into the network's learning process. A sliding window strategy reduces data acquisition costs by extracting training samples from a small amount of full-wave simulation data. While the CNN-based approach of An et al. captures coupling through local neighborhoods with fixed connectivity, the GNN framework of Wu et al. naturally accommodates arbitrary spatial relationships and varying numbers of neighbors, offering greater flexibility for modeling large-scale metasurfaces with complex coupling topologies. Microwave experiments confirmed the effectiveness of this GNN framework in practical scenarios.

3.2. Inverse Design of Static Metasurfaces

Phase modulating: The inverse design of phase-modulating metasurfaces has been addressed through three distinct methodological paradigms, each targeting different bottlenecks in the design workflow.

The first paradigm employs RL to navigate vast discrete design spaces without requiring pre-computed datasets. Sajedian et al. employed a Double Deep Q-Network (DDQN) to optimize the structural parameters of multilayer metasurface holograms [37]. The designed transmission-type, polarization-independent hologram operating in the visible regime achieved a transmission efficiency nearly twice that of previously reported results, demonstrating the effectiveness of RL for metasurface optimization.

The second paradigm replaces pre-generated datasets with physics-driven training. Chen et al. proposed a physics-driven generative neural network for the design of nearly dispersionless multicolor beam deflectors for near-eye display applications [82]. By embedding an electromagnetic solver as an integral part of the training process, their model learns to directly generate structures with high diffraction efficiency from randomly sampled noise, bypassing the time-consuming step of dataset generation. The designed in-coupling metagratings achieved an absolute diffraction efficiency exceeding 89%. Along a similar direction, Jiang and Fan proposed GLOnet, a conditional generative neural network that performs global optimization of dielectric metasurfaces without requiring pre-computed training datasets [113]. Unlike local adjoint-based topology optimization, which is sensitive to initial conditions, GLOnet initially generates a device distribution broadly sampling the design space and then refines this distribution toward high-efficiency regions over the course of training.

The third paradigm leverages transfer learning to reduce data acquisition costs. Zhu et al. transferred the Inception V3 model, originally developed for image recognition, to metasurface design [83]. By treating meta-atoms as images and retraining with a limited amount of domain-specific data, the network predicted the reflection phase of meta-atoms with an accuracy of approximately 90% as shown in Figure 3b. Fan et al. further advanced this direction by developing a transfer-learning-assisted inverse design framework that integrates an encoder–decoder architecture with a Physics-Assisted Network (PAN) grounded in antenna array theory [84]. The encoder–decoder establishes an inverse mapping from the desired far-field pattern to the phase distribution, while the PAN provides forward modeling constraints, effectively resolving the one-to-many non-uniqueness issue. This framework achieves over 30% savings in training data while maintaining design accuracy, establishing a data-efficient and transferable inverse design paradigm for far-field functionality customization.

Amplitude modulating: The inverse design of amplitude-modulating metasurfaces has been explored through generative models, end-to-end mapping, and search-based strategies, each offering distinct advantages for different design scenarios.

GANs have demonstrated particular strength in overcoming parametric design constraints. So and Rho pioneered the application of conditional deep convolutional GANs (cDCGAN) to the inverse design of nanophotonic antennas, enabling the generation of novel freeform structures with desired optical properties beyond predefined geometric templates [88]. Addressing the need for end-to-end automation, Qiu et al. proposed the "REACTIVE" method that combines an autoencoder with a FCNN to establish a direct mapping from target S-parameters to unit cell configurations [89]. Once trained, the model accepts arbitrary target electromagnetic properties as input and automatically generates the corresponding metasurface structure, reducing the need for specialized domain expertise.

As an alternative to training explicit inverse networks, Nadell et al. introduced the fast forward dictionary search (FFDS) strategy [90]. This approach trains only a high-accuracy forward prediction network and then rapidly searches through a pre-sampled structural library to identify the geometry whose predicted spectrum best matches the target. By leveraging the uniqueness of forward mapping, this method fundamentally circumvents the difficulty of approximating multi-valued inverse mapping relationships.

Ghorbani et al. [114] extended inverse design to the ultra-wideband regime (4–45 GHz), training a DNN to generate metasurface patterns from specified reflection spectrum requirements with an average prediction accuracy exceeding 90%. Beyond purely data-driven networks, physics-guided approaches have also been explored for absorber inverse design. Wu et al. proposed an equivalent-circuit-intervened deep learning framework that combines transmission line theory with a deep neural network and an improved genetic algorithm for the inverse design of microwave absorbers as shown in Figure 3e [109]. By using equivalent-circuit modeling to constrain the impedance prediction and then refining the geometry through genetic algorithm optimization, the method achieved single-layer notched-band, dual-layer trap, and triple-layer ultra-wideband absorbers based on indium tin oxide films, demonstrating that embedding physical priors can significantly reduce data dependency and improve interpretability for absorber design.

The above absorber designs operate under fixed material parameters. A complementary line of work has extended AI-driven inverse design to tunable terahertz absorbers, where graphene and vanadium dioxide (VO_2) introduce additional electrical and thermal degrees of freedom and substantially enlarge the design space. Conventional approaches based on full-wave simulation combined with equivalent-circuit modeling can capture the multi-band response of graphene split-ring resonators with multiple gaps and connecting bars [115], but become increasingly intractable as the number of tunable parameters grows. The complexity of multi-band, polarization-sensitive graphene THz absorbers motivates the application of data-driven inverse design methods. Ding et al. employed an artificial neural network (ANN) to inversely design a composite graphene-based metasurface absorber achieving 96.33% absorption across the quasi-entire 0.5–10 THz range, with the ANN enabling rapid parameter selection over a design space that would be prohibitive to traverse manually [116]. Kiani et al. extended this idea to dynamically tunable graphene metasurfaces, training two CNNs via transfer learning to jointly predict the passive geometric structure and the chemical-potential distribution required for on-demand reconfigurable responses, thereby unifying static structure design and active tunability within a single AI workflow [117].

Polarization modulating: The intricate coupling mechanisms and vast design degrees of freedom inherent in multi-element metasurfaces pose significant challenges that conventional optimization methods struggle to overcome. Two representative approaches illustrate contrasting strategies for managing this complexity.

Liu et al. proposed a hybrid AI framework integrating a Compositional Pattern-Producing Network (CPPN) with Cooperative Coevolution (CC), achieving the inverse design of metamolecules for arbitrary manipulation of polarization and wavefront as shown in Figure 3c [92]. The core idea lies in decomposing the global design task of metamolecules into independent optimization subproblems for individual meta-atoms. The CPPN encodes high-dimensional meta-atom structures into a low-dimensional latent space, and the CC algorithm iteratively optimizes the latent vectors of each meta-atom in a round-robin fashion. This strategy effectively avoids the exponentially growing full-wave simulations required for enumerating all possible combinations. This work demonstrates the potential of combining deep learning with evolutionary algorithms to solve high-dimensional inverse design problems in photonics.

In contrast to this divide-and-conquer approach, Zhu et al. [93] proposed a multiplexing neural network (MNN) that exploits physical-layer decoupling to simplify the problem at its root. By leveraging the physical principles of orthogonality and helicity decoupling, the originally coupled multi-parameter control problem is reduced to multiple independent one-to-one mappings so that a simple three-layer neural network suffices for each channel. As validation, the study integrated four functions, namely scattering, anomalous reflection, focusing, and holography, within the same metasurface aperture, with both simulation and experimental results in excellent agreement with the design targets. Compared to Liu et al.'s framework, which handles complexity through computational decomposition, the

https://doi.org/10.3390/aimater1020005

MNN approach reduces complexity through physical insight, resulting in substantially simpler network architectures.

Multifunctional metasurface: Beyond single-functionality design, recent work has explored AI-driven approaches for metasurfaces that simultaneously serve multiple functions.

Fan et al. introduced the concept of a "meta-disk" that uses the relative rotation angle between two stacked metasurfaces as a tunable physical weight [94]. They constructed a Twisted Diffractive Neural Network (TDNN) to simulate the optical field propagation process and through the inverse design of the metasurface phase distribution, the system outputs corresponding target images at different twist angles. This research provides a novel paradigm for optical holographic storage with significantly expanded capacity.

Huang et al. [95] addressed the need for rapid development of terahertz absorbers by proposing a hybrid method that integrates simulated annealing (SA) with deep learning acceleration. A forward neural network first establishes a quantitative mapping between geometric parameters and the absorption spectrum, and then serves as a fast evaluator within the SA algorithm to inversely search for optimal parameters. By exploiting the insulator-to-metal phase transition property of VO_2, the designed broadband absorber achieves switchable modulation between broadband and triple-band absorption modes.

Zhang et al. proposed a multipole-decomposition-guided adjoint method for multifunctional metasurface inverse design as shown in Figure 3f [111]. By decomposing the scattered field into independent electric and magnetic multipole contributions and formulating the design objective directly in terms of these components, the adjoint method provides analytical gradients for simultaneously optimizing multiple functional channels within a single metasurface. This physics-decomposed strategy reduces the dimensionality of the inverse problem and complements purely data-driven generative approaches.

Li et al. introduced MetaAI, a physics-aware current-diffusion framework for metasurface structure discovery [118]. Rather than directly mapping target responses to structural layouts, MetaAI generates intermediate electrical current distributions as a physical bridge between electromagnetic performance and metasurface topology through a dual-domain diffusion module operating in both spatial and frequency domains. This approach enables extrapolation to unexplored performance regimes beyond the training distribution, discovering non-intuitive structures with 17.2% wider operational bandwidths.

3.3. Inverse Design of Reconfigurable Metasurfaces

Reconfigurable metasurfaces represent a qualitatively different design challenge compared to their static counterparts. Rather than a one-time optimization, they require real-time closed-loop control in which the metasurface configuration must adapt to dynamically changing environments within millisecond time scales. This section reviews AI-driven approaches for three representative application domains of reconfigurable metasurfaces.

Invisibility cloak: Conventional invisibility cloaks are limited by static designs and predetermined illumination conditions, making it difficult to cope with dynamically changing incident waves and complex backgrounds. The development of intelligent cloaking has progressed through three stages, from single-surface adaptive cloaking to three-dimensional large-scale systems and ultimately to mobile platforms.

Qian et al. proposed the concept of a deep learning-driven intelligent self-adaptive invisibility cloak with a tunable metasurface [96]. By embedding a pre-trained ANN and independently tuning the reflection characteristics of each meta-atom via varactor diodes, the metasurface cloak can autonomously respond to varying incident waves and surrounding environments on a millisecond timescale without human intervention. This work laid the foundation for real-time, in situ cloaking applications.

Scaling this concept to three dimensions, Wang et al. proposed a universal framework for 3D intelligent cloaking devices and experimentally demonstrated a large-scale intelligent cloaked vehicle equipped with thousands of reconfigurable full-polarization metasurfaces [97]. Their hybrid inverse design framework combines a forward DNN for rapid scattering field prediction with a local optimization algorithm for searching the optimal configuration within the vast solution space.

Qian et al. further extended intelligent invisibility to aeroamphibious scenarios on an unmanned aerial vehicle platform [98]. They introduced the generation-elimination network, consisting of a cVAE for generating candidate solutions and a forward neural network for eliminating inferior ones, effectively addressing the non-uniqueness issue while rapidly outputting control instructions. In experiments, a fully functional invisible drone flew through a conical detection region with nearly zero backscattering, extending the invisibility cloak family to the flying modality.

Wireless communication: AI-driven reconfigurable metasurfaces have been increasingly applied to dynamic wireless channel management, progressing from global channel control to real-time beam tracking and broadband adaptive design. Fan et al. proposed a homeostatic neuro-metasurface architecture for autonomous dynamic channel control as shown in Figure 3d [99]. They combined mechanically driven reconfigurable metasurfaces with deep learning, employing a CNN-based encoder–decoder architecture for global inverse design where the reflection phase of each meta-atom is individually adjusted via mechanical rotation. Li et al. [100] extended this concept to real-time scenarios by integrating computer vision (YOLOv4-tiny) with digital programmable metasurfaces (DPMs), achieving simultaneous intelligent electromagnetic tracking and communication in a closed-loop mode without human intervention.

Building on this vision-integrated paradigm, Zhang et al. demonstrated a holographic communication system that integrates a depth camera, a modified YOLOv5s target detection algorithm, software-defined radio modules, and a spin-decoupled programmable coding metasurface, with the metasurface configurations decoded in real time through a modified Gerchberg–Saxton algorithm as shown in Figure 3g [110]. Target information is acquired and encoded in the optical domain, transmitted via long-term evolution at 5 GHz, and finally reproduced as holographic images at 12 GHz by the reconfigurable metasurface, illustrating an end-to-end intelligent scheme that converts optical information into electromagnetic wavefronts and bridges AI-driven sensing with metasurface-based wireless communication.

Addressing the challenge of slow beam control response, Wen et al. proposed a real-time reconfigurable microwave reflective surface driven by real experimental data [101]. Their sequential tandem neural network architecture combines CNNs as forward predictors with RNNs as inverse designers capable of outputting control voltages in real time. A distinctive feature of this work is that the networks were pre-trained using actual experimental data, effectively avoiding errors introduced by simulation or manufacturing tolerances.

For large-scale, shape-varying metasurfaces, Jia et al. [102] introduced a knowledge-inherited learning paradigm based on a "parent-offspring" assembly framework. The metasurface is treated as an "offspring" structure assembled from multiple "parent" panels, with inherited neural networks (INNs) capturing the electromagnetic response of each panel and an assembled neural network decomposing the global objective into local responses. This approach significantly reduces design dimensionality and data dependency. Jia et al. [103] subsequently extended this framework by proposing a synthetical neural network that actively models the electromagnetic coupling effects between components, improving broadband design capability and overall accuracy.

Sensing and adaptive focusing: The integration of deep learning with reconfigurable metasurfaces has also enabled intelligent sensing and adaptive focusing systems that operate autonomously in complex electromagnetic environments.

Li et al. [104] proposed a ML reprogrammable metasurface imager that combines deep learning with a reconfigurable 2-bit coding metasurface for microwave imaging. By introducing methods such as Principal Component Analysis (PCA) and random projection, the system learns the optimal measurement modes required for specific tasks and inversely calculates the corresponding coding states, achieving scene perception and recognition capabilities. This pioneering work established a technological paradigm for compressed imaging applications at microwave, millimeter-wave, and terahertz frequencies.

Two subsequent works by Lu et al. demonstrate complementary strategies for adaptive focusing. The first, inspired by the accommodation mechanism of the human eye, introduces Supervised Evolving Learning (SEL) [105]. This algorithm progressively approximates the focal point by continuously adjusting metasurface voltages, while a memory module stores real-time data and periodically retrains the Focus Steering Network (FSN), enabling the network to evolve and adapt to environmental changes. The system has demonstrated robust adaptive focusing capabilities across various scenarios including different incident angles, dual-source interference, and obstacle occlusion.

The second approach employs the deep reinforcement learning algorithm Soft Actor-Critic (SAC) to drive a reconfigurable metasurface for focusing through obstacles [106]. The agent collects real-time electric field data from the focal plane, and the actor-critic framework progressively optimizes the metasurface configuration to match a preset target distribution. This architecture exhibits excellent adaptability and robustness in unknown multi-obstacle scenarios, offering a promising technical approach for addressing signal penetration challenges in future wireless communications.

Across the forward modeling efforts reviewed above, a clear methodological progression is visible. Early approaches based on feedforward networks and parametric inputs have given way to architectures that handle freeform geometries through image-based CNNs, capture spectral correlations through sequential models such as LSTMs and RNNs, and account for inter-unit coupling through GNNs. The shift from predicting phase and amplitude directly to predicting complex transmission coefficients [40] has become a widely adopted strategy for circumventing resonance-induced discontinuities.

On the inverse design side, a rich toolkit has been developed to address the non-uniqueness problem from different perspectives. Tandem networks enforce forward consistency [33], generative models produce diverse solution candidates [88], physics-driven training eliminates the need for pre-computed datasets [82], and transfer learning reduces data requirements for new design tasks [83,84]. For reconfigurable metasurfaces, the design challenge extends beyond static optimization to real-time closed-loop control. The progression from single-surface adaptive cloaking [96] to three-dimensional mobile platforms [97,98] and from static beam design to real-time data-driven beam steering [101] illustrates the rapid maturation of this subfield.

Despite this progress, several challenges persist. Most current approaches treat individual meta-atoms or small neighborhoods independently, and scalable methods for end-to-end design of complete large-scale metasurfaces remain limited. The coupling-aware approaches of An et al. [107] and Wu et al. [112] represent important steps, but extending these to full-device optimization with millions of elements remains an open problem. Furthermore, experimental validation of AI-designed metasurfaces, particularly for reconfigurable systems, is still concentrated in the microwave regime, and extending these demonstrations to optical frequencies will require addressing additional challenges in fabrication precision and real-time tunability.

4. Periodic and Guided-Wave Photonic Structures

Periodic photonic structures represent a distinct class of metamaterial platforms where Bloch wave interference and photonic bandgaps govern the electromagnetic response. At the most fundamental level, one-dimensional periodic structures such as multilayer thin films and distributed Bragg reflectors (DBRs) exploit quarter-wavelength interference to achieve high reflectivity or tailored spectral filtering, serving as essential building blocks in optical coatings, laser cavities, and spectral filters. As dimensionality increases, PCs emerge as periodic dielectric structures characterized by spatially modulated refractive indices, giving rise to photonic bandgaps where electromagnetic wave propagation is forbidden within specific frequency ranges [54]. The photonic band structure, determined by the eigenvalue problem of Maxwell's equations in periodic media, exhibits a complex dependence on unit cell geometry, lattice symmetry, and material composition [119]. Periodic photonic structure design therefore involves discrete structural variables constrained by lattice symmetry and periodicity, creating unique challenges for neural network-based optimization.

It is worth noting that while periodicity defines a major class of photonic structures, AI-driven design methodologies developed for periodic systems naturally extend to compact guided-wave components such as power splitters, waveguide crossings, and mode converters. These non-periodic devices share common design challenges with periodic structures in terms of high-dimensional parameter spaces and complex electromagnetic responses. Grating couplers, as periodic diffractive structures designed to couple free-space light into waveguides, serve as a natural bridge between periodic photonic elements and compact guided-wave components in terms of both physical functionality and AI design methodology. Accordingly, this chapter is organized into three sections according to the structural platform, each discussed in terms of forward modeling and inverse design.

The application of computational intelligence to photonic structure design predates the deep learning era. Preble et al. pioneered the use of genetic algorithms to design two-dimensional PCs as early as 2005, demonstrating that evolutionary optimization could discover non-intuitive geometries with enhanced bandgap properties [120]. This early work established the foundation for subsequent AI-driven approaches and highlighted the vast design space inherent in these periodic photonic platforms.

4.1. One-Dimensional Periodic Structures

One-dimensional periodic photonic structures, including multilayer thin films, distributed Bragg reflectors, and periodic grating structures, represent the simplest form of periodic photonic media. Their optical responses are governed by thin-film interference or diffraction, with design parameters typically limited to layer thicknesses, material choices, and grating geometries. This relatively low-dimensional design space makes them natural starting platforms for developing and validating neural network-based design methodologies. The design objectives for these systems encompass broadband high reflectance or absorption, diffraction control, coupling efficiency maximization, and spectral filtering.

4.1.1. Forward Modeling

Neural networks have been applied to model the optical responses of one-dimensional periodic grating structures. Tu et al. systematically investigated DNN architectures for silicon photonic grating couplers, demonstrating that forward modeling networks can predict coupling efficiency spectra with high accuracy while enabling rapid design space exploration [121]. Their comprehensive study on network hyperparameters, including hidden layer depth, node count, and training strategies, established practical guidelines for applying DNNs to wavelength-sensitive periodic photonic devices.

4.1.2. Inverse Design

Multilayer thin film design: Liu et al. introduced the tandem neural network architecture to address the fundamental non-uniqueness problem in photonic inverse design as shown in Figure 4a, where multiple distinct structures can produce identical optical responses [33]. This seminal work on alternating dielectric thin films established a widely adopted framework for subsequent photonic inverse design studies.

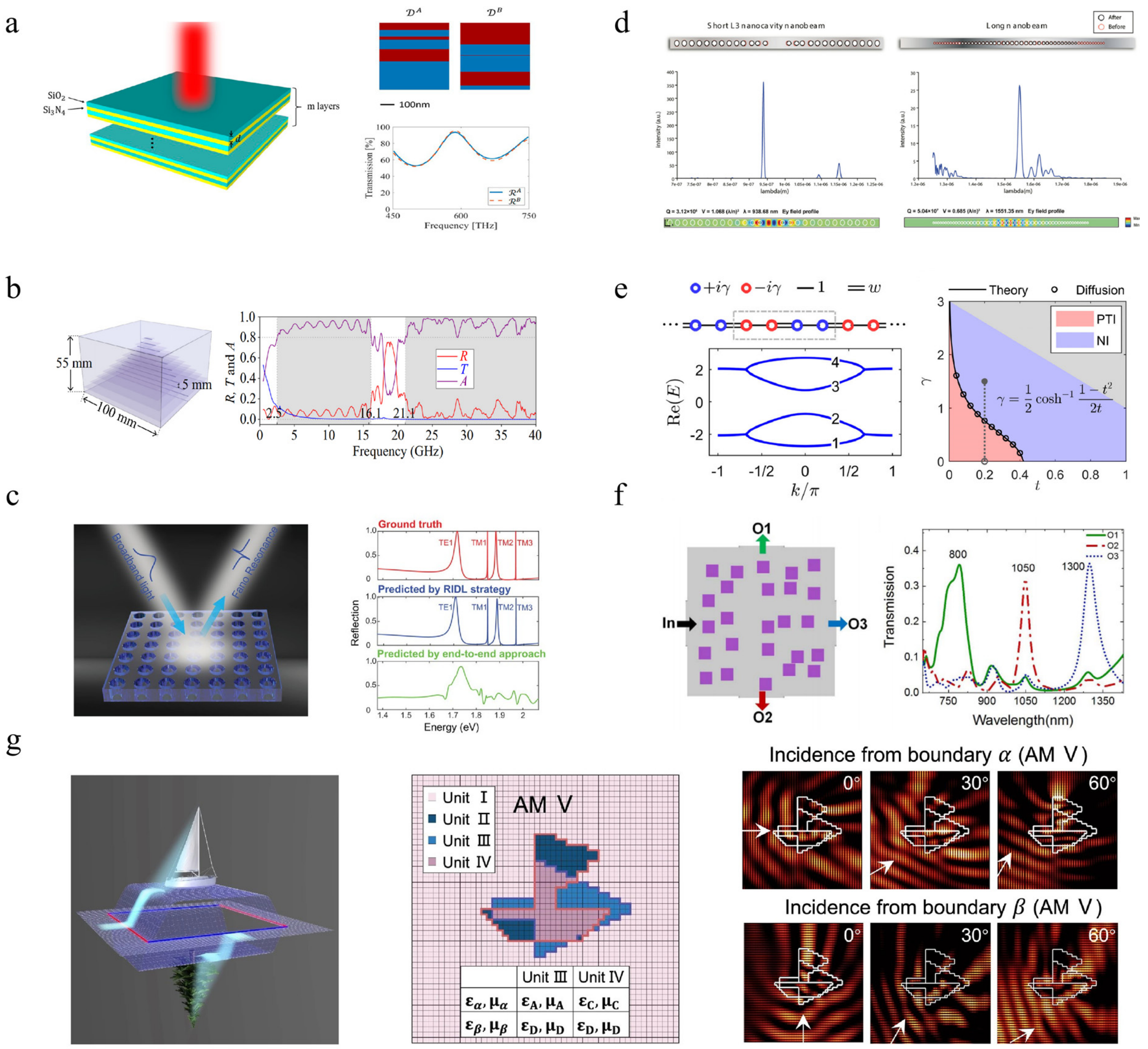

Figure 4. (**a**) Schematic of the multilayer thin-film stack (**left**), two distinct layer-thickness solutions D^A and D^B generated by the tandem network for the same target (**top right**), and transmission spectra R^A and R^B of the two designs (**bottom right**) (reproduced from [33]). (**b**) Fabricated pyramidlike multilayer ITO absorber exploiting the anomalous Brewster effect (**left**), and measured reflection, transmission, and absorption spectra showing broadband high absorption across 2.5–16.1 GHz and 21.1–40.0 GHz (**right**) (reproduced from [122]). (**c**) Schematic of the high-Q photonic crystal slab supporting symmetry-protected bound states in the continuum (**left**), and comparison between the ground-truth reflection spectrum and spectra predicted by the RIDL strategy and an end-to-end approach (**right**) (reproduced from [123]). (**d**) Resonance spectra and optimized air-hole configurations of L3 and nanobeam photonic crystal cavities before and after L2DO training, achieving Q factors of 3.12 × 10^6 and 5.04 × 10^7, respectively (reproduced from [124]). (**e**) Unit cell of the non-Hermitian CROW system with balanced gain and loss rings (**left top**), real part of the quasiband structure (**left bottom**), and theoretical phase boundary (solid curve) compared with the diffusion-

map results (open circles) separating the PTI and NI phases (**right**) (reproduced from [125]). (**f**) Freeform silicon wavelength router optimized by a genetic algorithm coupled with FEM simulations (**left**), and transmission spectra at output ports O1, O2, and O3 showing selective routing of 800, 1050, and 1300 nm wavelengths (**right**) (reproduced from [126]). (**g**) Two optical spaces containing a boat-shaped scatterer and a tree-shaped scatterer realized as photonic multiple realities (**left**), configuration of artificial material AM V composed of four types of units (**middle**), and intensity distributions $|E_z|^2$ under Gaussian beam incidence from boundaries α and β at 0°, 30°, and 60° (**right**) (reproduced from [127]).

To further address the multimodal nature of inverse design solutions, Unni et al. developed mixture density networks (MDNs) that model design parameters as probability distributions rather than deterministic values [128]. This probabilistic approach explicitly captures the degeneracy in structure-to-spectrum mappings and provides multiple viable design candidates for a given target response. Building on this foundation, the same group demonstrated mixture-density-based tandem optimization networks for designing 20-layer thin-film high reflectors with extended high-reflectance zones, reproducing designs derived from physical principles with high precision and enabling improved designs beyond the reach of conventional methods [129].

Most recently, transformer-based architectures have been introduced to multilayer thin film design. Ma et al. proposed OptoGPT, a transformer that reformulates inverse design as a sequence generation problem [130]. By tokenizing material choices and layer thicknesses into discrete sequences, OptoGPT can autonomously determine both material selection and thickness optimization across layers, accommodating design spaces exceeding 10^{59} possible configurations. This foundation model approach represents a paradigm shift from structure-specific neural networks toward more generalizable design frameworks capable of handling diverse materials, angles, and polarization states within a unified architecture.

Zhang et al. proposed a recurrent neural adjoint (RNA) method for multilayer optical filter inverse design, treating each layer as a step in a sequence so that the recurrent architecture captures inter-layer correlations while the adjoint method provides efficient thickness gradients [131]. The approach was demonstrated on solar simulator filters matching the air mass 1.5G reference spectrum, with Si_3N_4/SiO_2 and Ta_2O_5/SiO_2 stacks operating across the 280–800 nm and 280–1350 nm bands, illustrating the value of pairing sequence-aware architectures with physics-informed gradient methods for broadband multilayer design.

In addition to spectral design, DNN optimization has been applied to multilayer metamaterial absorbers with experimental validation. Jing et al. [122] demonstrated ultrabroadband transparent metamaterial absorbers consisting of pyramidlike multilayered indium tin oxide (ITO) films, exploiting the anomalous Brewster effect and gradient impedance matching for high-efficiency absorption as shown in Figure 4b. To further optimize the absorption bandwidth, the separation distances between ITO films were treated as design variables and optimized using a trained forward DNN combined with the neural adjoint method. This optimization extended the high-absorption band to cover 1.7–40.0 GHz with an average absorptance exceeding 93%, and the design was experimentally validated in the microwave regime. This work provides an example of closed-loop integration between neural network optimization and experimental realization for periodic multilayer structures.

Shao et al. further advanced physics-inspired architectures for multilayer photonic structures by proposing the electromagnetic neural network (EMNN) [132]. EMNN consists of two components: EMNN Netlet, which serves as a local electromagnetic field solver by encoding both electromagnetic field information and diffraction modulation into complex tensors with physics-inspired linear connections, and Huygens-Fresnel Stitch, which concatenates local predictions based on the Huygens-Fresnel principle to handle structures of arbitrary size. This decomposition strategy enables scalable inverse design of multilayer on-chip computing metasystems without retraining when the number of layers changes. Under identical training conditions, EMNN demonstrated superior predictive accuracy compared to non-physics-inspired networks, highlighting the value of embedding wave propagation physics into network architecture for multilayer photonic design.

Grating and grating coupler design: Tu et al. demonstrated that inverse DNN models can efficiently design silicon photonic grating couplers, directly predicting structural parameters from target spectral responses [121]. Their systematic analysis revealed the trade-offs between network complexity and design accuracy, providing a foundation for neural network-based grating optimization.

Generative neural networks have emerged as powerful tools for designing complex grating topologies with freeform geometries. Jiang et al. proposed a conditional generative adversarial network (cGAN) platform for free-form diffractive metagrating design [42]. The generator network learns from images of topology-optimized metagratings to produce high-efficiency structures capable of large-angle beam deflection across broad wavelength ranges. This hybrid approach, combining GAN-based generation with subsequent local optimization, achieves diffraction efficiencies comparable to computationally expensive topology optimization while significantly reducing the overall computational cost compared to conventional topology optimization alone.

Hooten et al. introduced PHORCED (Photonic Optimization using REINFORCE Criteria for Enhanced Design), a reinforcement learning approach using policy gradients for grating coupler inverse design [133]. Unlike supervised learning methods that require pre-computed training datasets, PHORCED interfaces a probabilistic generative neural network directly with electromagnetic simulations, learning optimal design strategies through iterative feedback. The method achieved superior coupling efficiency compared to adjoint-based local optimization while demonstrating effective transfer learning capability, highlighting the potential for rapid design iteration across device families.

4.2. Two- and Three-Dimensional Photonic Crystals

Two- and three-dimensional PCs present substantially greater design complexity than their one-dimensional counterparts. The photonic band structure in these systems is determined by the eigenvalue problem of Maxwell's equations in periodic media, exhibiting a complex dependence on unit cell geometry, lattice symmetry, and material composition [119]. The design objectives span multiple physical properties, including complete or partial photonic bandgaps for waveguiding and filtering [134], group velocity profiles for slow light generation [135], quality factors for nanocavity design [136], and symmetry-protected edge states for topological light transport [12]. Each objective presents distinct optimization landscapes and requires tailored neural network strategies.

4.2.1. Forward Modeling

Band Structure Prediction: Early work by Ferreira et al. demonstrated that multilayer perceptrons (MLPs) and extreme learning machines (ELMs) can accurately predict dispersion relations and photonic bandgaps in two- and three-dimensional PCs [55]. Using datasets generated from an electromagnetic solver, the trained networks achieved rapid prediction of band structures from geometric parameters, establishing the feasibility of neural network surrogates for eigenvalue problems in periodic systems.

Subsequent advances have incorporated physics-informed deep learning to improve both accuracy and interpretability of band structure prediction. Katsikas et al. embedded a rigorous tight-binding model as a known operator within a deep neural network for predicting the optical properties of two-dimensional photonic crystals [137]. Rather than learning the high-dimensional full electromagnetic response directly, this approach predicts physically meaningful tight-binding parameters.

Q-factor Prediction for Nanocavities: Asano and Noda pioneered the application of CNNs to predict Q-factors of two-dimensional photonic crystal nanocavities [138]. The network architecture comprised one convolutional layer followed by three fully connected layers, taking displacement vectors of air holes surrounding a line defect as input. Trained on datasets generated by numerical simulations, the CNN achieved excellent correlation between predicted and simulated Q-factors, demonstrating the capability of deep learning to capture the relationship between structural perturbations and radiation loss.

Ma et al. developed a strategic deep learning approach specifically designed for high-Q photonic crystal slabs supporting bound states in the continuum (BICs) as shown in Figure 4c [123]. Unlike methods that directly predict spectral responses, this network first decomposes spectra using an adaptive data acquisition method. It incorporates resonance information to predict both the smooth background spectra and the resonance parameters in Fano equations. These components are then combined to reconstruct the full spectra. Applied to symmetry-protected BICs on suspended silicon nitride photonic crystal slabs, this physics-informed decomposition achieves high-accuracy prediction using considerably small training datasets, with experimentally validated angle-resolved band structures showing minimal differences from predictions.

Dispersion Prediction: For photonic crystal waveguide design, neural networks have been applied to predict group index and dispersion characteristics essential for slow light applications. Pavan et al. proposed feedforward neural networks to predict dispersion relations and group indices of dispersion-engineered photonic crystal waveguides, achieving rapid evaluation compared to conventional PWE simulations [139]. Hirotani et al. combined ML with band structure modeling to optimize silicon photonic crystal waveguides, achieving a normalized delay-bandwidth product of 0.45, close to the theoretical upper limit, with group indices around 20 across the full C-band [140].

4.2.2. Inverse Design

Bandgap Optimization: The inverse design of PCs for specified bandgap properties has been addressed through multiple deep learning paradigms. Ma et al. employed tandem networks to inversely design two-dimensional PCs with large complete photonic bandgaps (CPBGs), addressing the non-uniqueness problem inherent in structure–property mappings [141]. Their work revealed that the connecting channel between the primitives in the photonic crystal unit cell has a dominant effect on the CPBG, providing physical insight alongside optimized designs.

Notably, gradient-based inverse design leveraging automatic differentiation has also emerged as a powerful approach for bandgap engineering. Minkov et al. [142] implemented PWE and guided-mode expansion methods within automatic differentiation frameworks, and Luce et al. [143] further advanced this direction by merging automatic differentiation with the adjoint method. While these approaches share the mathematical machinery of backpropagation with deep learning, they are fundamentally deterministic gradient-based optimization methods rather than learned models. They are included here to provide a complete picture of the computational design landscape.

Most recently, Cui et al. proposed a universal periodic structural design method based on deep learning-assisted inverse Fourier transform, which enables the creation of arbitrary geometries within crystallographic space groups [144]. Applied to three-dimensional PCs, the approach modeled numerous structures and identified their photonic bandgaps within hours, confirming the supremacy of the single diamond network and uncovering a rarely known lcs topology with excellent photonic properties.

High-Q Nanocavity Design: The inverse design of high-Q photonic crystal nanocavities represents a particularly challenging optimization problem due to the sensitivity of Q-factors to structural perturbations. Building on their forward modeling work, Asano and Noda extended their CNN approach to inverse design by iteratively optimizing air hole displacements, achieving Q-factors exceeding 11 million [138,145].

Li et al. proposed Learning to Design Optical-Resonators (L2DO), a deep reinforcement learning framework combining Deep Q-learning and Proximal Policy Optimization algorithms for autonomous nanocavity optimization as shown in Figure 4d [124]. Unlike supervised learning approaches requiring large pre-computed datasets, L2DO learns through interaction with electromagnetic simulators, addressing three critical limitations in conventional approaches: data scarcity, one-to-many mapping ambiguity, and the inability to surpass training data performance. Trained for less than 152 h on limited hardware resources, L2DO achieved Q-factors exceeding 50 million while simultaneously optimizing resonance frequency and modal volume.

Liu and Long recently proposed an intelligent model for efficient data augmentation that requires merely a few hundred original samples, tackling the challenge of data scarcity in high-Q microcavity designs [146]. This work exemplifies the broader trend of developing data-efficient strategies for photonic design, as generating large-scale datasets for complex eigenvalue problems remains computationally prohibitive [67]. Their novel structural reshaping strategy, involving Euler-bend air-hole structures, significantly enhances fabrication robustness, addressing the consistency challenge associated with large-scale manufacturing of high-Q photonic crystal microcavity arrays. Experimentally demonstrated silicon photonic crystal nanobeam cavities achieved record loaded Q factors with large tolerance for Euler-bend holes and extremely compact sizes of 6 μm^2.

Dispersion Engineering and Slow Light Waveguides: The inverse design of photonic crystal waveguides for slow light applications requires optimizing multiple geometric parameters to achieve flat dispersion bands with high group indices. Yan et al. applied deep RL to design slow-light photonic crystal waveguides, obtaining structures with normalized delay-bandwidth products of 0.449 and group indices of 48.72 within 72 h of training [147]. Compared to supervised deep learning approaches, RL improved sampling efficiency by over an order of magnitude while enabling designs beyond the performance envelope of pre-computed datasets.

Chen et al. advanced tandem network applications by designing photonic crystal waveguides with optimized dispersion profiles [57]. Their tandem classification regression neural network resolved data class imbalance issues and enabled rapid inverse prediction of waveguide geometric parameters from desired optical properties, achieving designs with a normalized delay-bandwidth product of 0.458 and a group index of 71. These results established tandem networks as effective tools for multi-parameter waveguide optimization.

Topological Photonic Structure Design: Topological photonic insulators supporting protected edge states have attracted significant attention for robust light transport applications. Long et al. demonstrated early on the application of ML to inverse design of photonic topological states, demonstrating that neural networks can map target Zak phases to structural parameters of one-dimensional PCs [148]. This early work established the feasibility of data-driven topological photonic design and motivated subsequent developments across higher-dimensional systems.

Singh et al. developed a deep learning framework to map the design space of topological states in PCs, overcoming dimensional mismatch between input (topological properties) and output (design parameters) through specialized network architectures [149]. The framework successfully reconciled the non-uniqueness arising from one-to-many function mappings, enabling on-demand design of PCs with specified topological invariants.

Pilozzi et al. addressed ML solutions to the topological inverse problem using the Aubry-Andre-Harper model [56]. By introducing a self-consistent cycle where tentative solutions are validated through forward network evaluation, their approach ensures physically viable designs while handling multivalued degeneracies inherent in topological systems.

Recent work has extended inverse design to valley-Hall photonic topological insulators. Wang et al. constructed tandem residual neural networks for multimodal inverse design, combining MLP-based parameter prediction with variational autoencoder-based structural image generation [150]. Residual connections accelerate training convergence while avoiding vanishing gradient problems. Full-wave simulations confirmed robust topologically protected wave propagation along designed domain walls with minimal backscattering. Yu and Hao proposed randomly encoded photonic crystal structures based on the SSH model, demonstrating wide bandgaps and topological corner states across diverse refractive-index platforms including III-V compounds and silicon nitride through deep learning-based inverse design [151].

Chen et al. demonstrated inverse design of second-order photonic topological insulators with multi-band corner states, employing topology optimization to produce four sizeable bandgaps each hosting highly localized corner states robust to bulk impurities [152]. The integration of ML with topological physics opens new avenues for designing photonic devices with enhanced robustness and functionality.

Beyond supervised learning approaches, Li et al. introduced unsupervised learning to identify the bulk topology of non-Hermitian photonic crystals without labeled training data [125]. By applying dimensionality reduction and clustering directly to spectral and eigenstate features, the framework autonomously distinguishes topologically distinct phases in systems with complex eigenvalues as shown in Figure 4e, where conventional Hermitian topological invariants are no longer applicable. This work extends AI-driven topological photonic design from Hermitian to non-Hermitian regimes and illustrates the potential of unsupervised learning for discovering topological phases that are difficult to characterize analytically.

Beyond topology-engineered functionalities, AI-driven photonic crystal design has also enabled the discovery of fundamentally new physical phenomena. Song et al. [127] employed DNNs combined with the neural adjoint method to inversely design two-dimensional photonic crystal unit cells whose equal-frequency contours (EFCs) are simultaneously shifted along orthogonal directions near the Brillouin zone boundary. By training DNNs to map unit cell geometry to the effective parameters of both optical spaces, the authors realized nonlocal artificial materials that support two independent effective media within a single physical structure, accessible through different material boundaries as shown in Figure 4g. This mechanism enabled experimental demonstrations of photonic wormholes as invisible optical tunnels and photonic multiple realities where two distinct scatterers coexist at the same location. This work demonstrates that AI-driven inverse design, by navigating parameter spaces inaccessible to human intuition, can reveal non-trivial photonic functionalities that were not anticipated by prior theoretical frameworks.

4.3. Compact Guided-Wave Components

As introduced at the beginning of this chapter, compact guided-wave components such as power splitters, waveguide crossings, and mode converters share methodological foundations with periodic structure design. Research in this area has focused primarily on inverse design, aiming to discover novel device topologies that meet target specifications within ultra-compact footprints.

Tahersima et al. pioneered DNN design of integrated photonic power splitters, demonstrating that DNNs can predict optical responses of arbitrary nanostructured topologies and inversely generate designs for target splitting ratios [153]. Their 2.6 $\times$ 2.6 μm^2 silicon devices achieved transmission efficiencies exceeding 90% with reflection below -20 dB, establishing neural network surrogates for freeform nanophotonic optimization.

Tang et al. advanced generative approaches by introducing cVAEs with adversarial censoring for nanopatterned power splitter design [154]. Their framework generates devices with arbitrary splitting ratios and ultra-broadband responses spanning 550 nm from compact 2.25 $\times$ 2.25 μm^2 footprints, demonstrating that generative models can efficiently explore vast design spaces while maintaining physical realizability.

Addressing training data efficiency, Ren et al. proposed a genetic algorithm combined with deep neural network (GDNN) hybrid approach requiring significantly less training data [155]. Applied to power splitters with uncommon splitting ratios, TE mode converters, and broadband splitters, GDNN-designed devices comply with silicon photonics fabrication design rules while achieving performance comparable to exhaustive optimization.

Beyond power splitters and mode converters, intelligent algorithms have also enabled the inverse design of more complex routing functionalities. Liu et al. realized an integrated nanophotonic wavelength router by combining a genetic algorithm with finite element method simulations to optimize a freeform silicon structure within a wavelength-scale footprint [126]. The designed router selectively directs different wavelengths into distinct output ports with high transmission efficiency, expanding AI-assisted compact device design from binary splitting toward wavelength-selective on-chip routing as shown in Figure 4f.

A critical advancement toward practical deployment came from Gostimirovic et al., who developed deep learning models for fabrication-aware inverse design [156]. Their tandem-trained corrector network learns proximity-dependent fabrication deviations from SEM images, enabling pre-compensation of lithographic errors. Experimental validation in a commercial silicon photonics foundry demonstrated inverse-designed devices with micrometer-scale footprints, marking a milestone for foundry-compatible AI-driven photonic design.

Periodic and guided-wave photonic structures present unique challenges for AI-driven design due to their discrete structural variables, symmetry constraints, and eigenvalue-based physical properties. The spectrum of platforms, ranging from one-dimensional multilayer thin films and gratings to two- and three-dimensional PCs and compact guided-wave components, demands tailored neural network approaches that respect their distinct design constraints and physical mechanisms.

From early evolutionary algorithms [120] to modern DL and RL paradigms, computational intelligence has progressively transformed the design methodology. The tandem neural network architecture [33] and its probabilistic extensions [128] first demonstrated effective strategies for handling the non-uniqueness inherent in all photonic inverse problems. A particularly important subsequent development is the emergence of data-efficient strategies, including physics-informed spectral decomposition [123] and intelligent data augmentation [146], which address the fundamental challenge of dataset generation for eigenvalue problems in periodic systems. Meanwhile, the extension of these methodologies to freeform guided-wave components [153,154] and fabrication-aware design workflows [156] has validated the generalizability of neural network approaches across both periodic and non-periodic photonic platforms. These advances have established periodic and guided-wave photonic structures as a mature platform for AI-assisted nanophotonic engineering, with continuing opportunities in more complex multi-objective optimization and closed-loop experimental validation.

5. Complex Scattering Systems

Complex scattering systems differ fundamentally from periodic or resonant photonic platforms in that light propagation is governed by high-dimensional multiple scattering and modal coupling rather than by a small set of well-defined resonant or Bloch modes. As the physical and electrical size of the system increases, waves undergo repeated scattering, mode mixing, and path-length diversity, giving rise to complex interference patterns that are highly sensitive to structural disorder and environmental perturbations. In such regimes, the input–output relationship between incident and transmitted fields is most naturally described by a high-dimensional transmission matrix (TM) [60,157]. The statistical properties of transmission matrices in disordered media have been extensively studied within the framework of mesoscopic wave physics and random matrix theory [58], revealing universal features that transcend specific microscopic realizations.

However, the dimensionality, randomness, absorption, and potential temporal variation in transmission matrices make direct measurement or analytical inversion increasingly challenging in realistic systems [58,60,157]. Neural networks therefore emerge as data-driven tools for approximating transmission matrices and their inverses, learning effective input–output mappings directly from experimental observations. Depending on the underlying physical mechanism, complex scattering systems can be broadly categorized into three classes. Multiple-scattering systems, such as opaque diffusers, are dominated by statistical TMs and have been explored through deep speckle-based modeling and reconstruction approaches [61,158,159]. Modal coupling systems, exemplified by multimode fibers, exhibit structured TMs arising from guided-mode mixing and dispersion, enabling learning-based transmission and imaging [66,159,160]. Dynamic and absorptive systems introduce additional absorption and temporal variability, leading to lossy and time-dependent TMs that have been addressed in deep learning-assisted microscopy and optoacoustic imaging [62,161–163]. Across these platforms, neural networks are typically applied in two fundamental roles: forward modeling of the transmission matrix to predict system responses, and inverse reconstruction or control to recover hidden objects, system parameters, or optimal excitation fields. In the following sections, we discuss each class in detail according to its dominant physical characteristics.

5.1. Multiple-Scattering Systems

In disordered scattering media such as opaque diffusers and random slabs, light undergoes multiple scattering without a stable and physically separable modal structure. The TM in such systems is a random high-dimensional matrix whose statistical properties can be analyzed within the framework of mesoscopic wave physics [58,60,157], and the output intensity forms seemingly random speckle patterns as shown in Figure 5a. It is worth noting that experimental techniques for probing these systems predate the deep learning era. Vellekoop and Mosk [164] pioneered iterative wavefront shaping to focus light through opaque scattering media in 2007, and Popoff et al. [60] subsequently introduced systematic transmission matrix measurement using spatial light modulators. These contributions established the experimental foundation upon which subsequent data-driven approaches have been built.

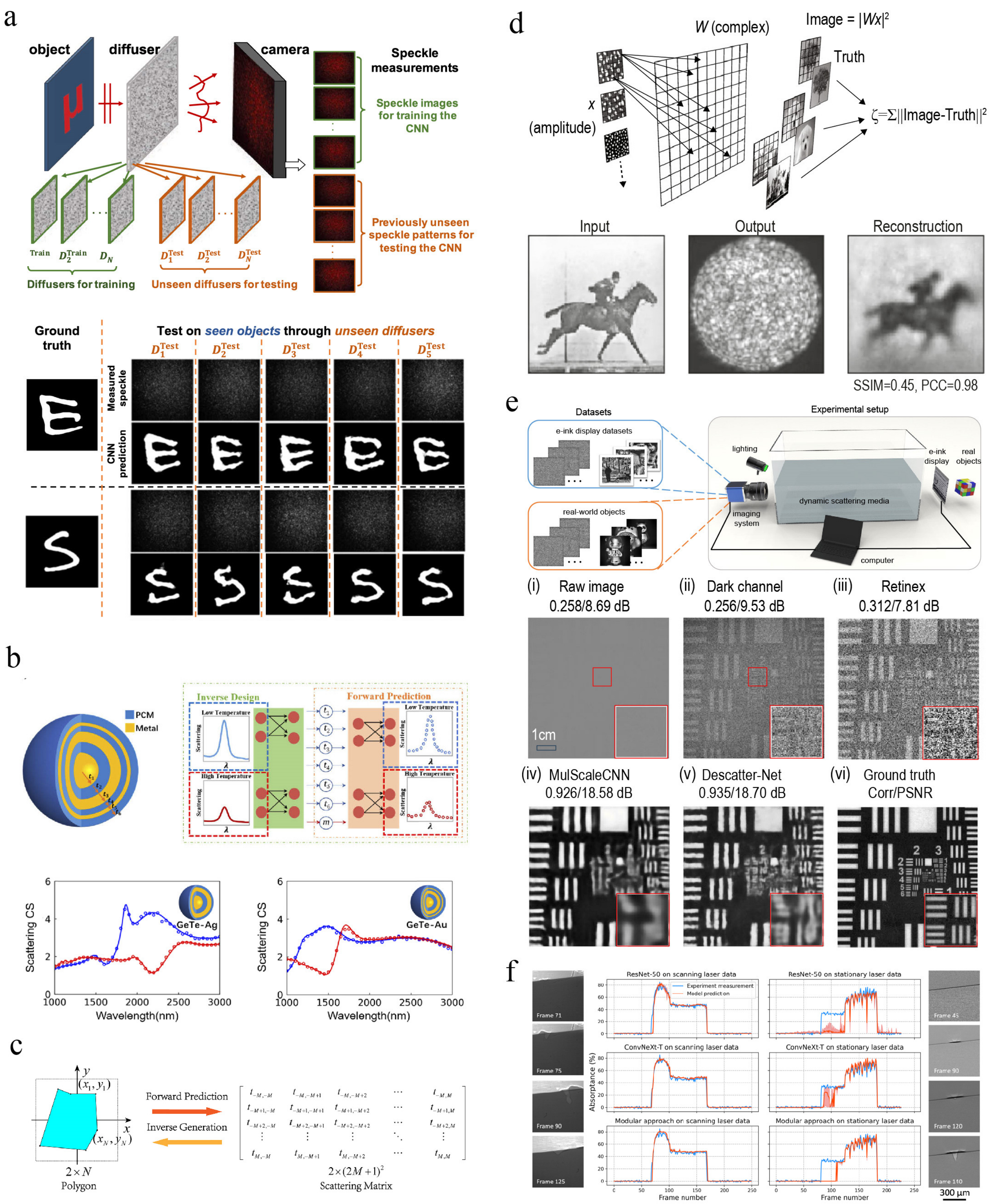

Figure 5. (**a**) Experimental configuration for deep learning-based imaging through scattering media using multiple diffusers (**top**), and reconstruction results for unseen diffusers demonstrating generalization capability (**bottom**) (reproduced from [61]). (**b**) Schematic of multilayer core–shell nanoparticles composed of phase-change materials and metals (**top**), and neural-network-assisted forward prediction and inverse design of scattering spectra enabling multi-wavelength switching between superscattering and invisibility (**bottom**) (reproduced from [165]). (**c**) Neural network-based forward prediction and inverse generation of scattering matrices for arbitrarily shaped two-dimensional

scatterers (reproduced from [166]). (**d**) Neural network-based modeling of light propagation in a multimode system with strong modal coupling (**top**), and comparison between input, speckle output, and reconstructed images (**bottom**) (reproduced from [160]). (**e**) Experimental setup for imaging through dynamic scattering media (**top**), and comparison of reconstruction results using conventional methods and neural network approaches (**bottom**) (reproduced from [162]). (**f**) Deep learning prediction of laser absorptance (reproduced from [163]).

5.1.1. Forward Modeling

Borhani et al. [159] demonstrated that DNNs can learn the mapping between input images and output speckle patterns in complex scattering systems. Instead of explicitly measuring the transmission matrix, the network implicitly approximated the high-dimensional TM. Their results showed that the learned model preserved sufficient statistical information to enable subsequent reconstruction, illustrating that the neural network captured the effective structure of the transmission matrix rather than memorizing patterns.

Rahmani et al. [66] extended this idea by modeling the nonlinear relationship between input phase or amplitude modulation and output speckle intensity in highly scrambled systems. Using CNNs, they achieved reconstruction fidelities approaching 98%, showing that spatial correlations embedded in the transmission matrix can be learned despite the apparent randomness of multiple scattering.

Fan et al. [167] addressed variability and randomness within disordered scattering environments, demonstrating that deep learning models can maintain predictive capability even when internal perturbations modify the transmission matrix. Compact network architectures were later shown to retain high reconstruction performance while significantly reducing computational complexity [168], indicating that the essential physics encoded in the TM can be compressed into relatively low-dimensional representations.

Beyond speckle prediction, neural networks have also been applied to estimate statistical scattering parameters, including transport mean free path, anisotropy factor, and absorption coefficient, from diffuse measurements [169]. These approaches can be interpreted as indirect inference of transmission matrix properties without explicit matrix reconstruction. In particular, such approaches enable the inverse design of nanoparticles exhibiting switching between superscattering and invisibility across multiple wavelengths [165], as shown in Figure 5b.

At a more fundamental level, DNNs have been applied to learn the full scattering matrix of individual scatterers. Jing et al. [166] developed a DNN that calculates the scattering matrix of arbitrarily shaped two-dimensional dielectric scatterers from their geometric coordinates, achieving speeds approximately 7500 times faster than finite element solvers, as shown in Figure 5c. This single-scatterer-level approach complements the complex-medium TM methods discussed above and provides a potential building block for hierarchical modeling of multiple scattering systems.

5.1.2. Inverse Reconstruction and Control

Imaging through scattering media: Li et al. [61] introduced the concept of deep speckle correlation imaging, where a CNN was trained across multiple diffusers with similar macroscopic parameters. Rather than learning a single fixed transmission matrix, the model captured statistical regularities of the TM, enabling generalization to unseen diffusers. This "one-to-all" strategy marked a significant departure from earlier approaches that required retraining for each individual scattering configuration.

Subsequent work using densely connected architectures achieved high-fidelity reconstruction through glass diffusers [158], demonstrating that deeper connectivity improves extraction of information embedded in the TM. Lyu et al. [170] further extended reconstruction beyond the optical memory-effect regime, showing that neural networks can compensate for the breakdown of conventional speckle correlation assumptions by effectively approximating the inverse TM.

GANs have been applied to reconstruct high-quality images from heavily degraded speckle measurements. Lai et al. [171] developed a Y-type GAN capable of simultaneously reconstructing images of multiple objects behind scattering media from a single speckle pattern, demonstrating the strong generalization ability of adversarial training for scattering inverse problems. Non-invasive imaging methods using dual-cycle GANs [172] have demonstrated the ability to work with unaligned training data, addressing practical limitations in real-world scenarios. Building on the physical principle of speckle correlations established by noninvasive focusing methods [173], physics-informed deep learning frameworks that embed memory effect constraints into network architectures or loss functions have further improved reconstruction robustness while reducing training data requirements.

Wavefront shaping and focusing: Wavefront shaping can be interpreted as solving for the inverse of the transmission matrix. Luo et al. [174] introduced genetic neural network (GeneNN), a hybrid algorithm combining DNNs with genetic algorithms, which first achieves preliminary focusing through a CNN and then refines the result via genetic optimization, demonstrating nearly doubled optimization speed and up to 40% improvement over conventional methods. The same group subsequently developed Timely-Focusing-Optical-Transformation-Net (TFOTNet) [64], a transfer-learning-empowered network for rapid optical refocusing through nonstationary scattering media, significantly reducing the time and computational cost of refocusing by leveraging speckle correlations between the medium's states before and after perturbation.

Turpin et al. [175] demonstrated that neural networks trained on pairs of binary intensity patterns and speckle measurements can predict wavefront corrections necessary to focus and scan light through opaque scattering media, bypassing iterative optimization procedures. Notably, their results revealed that neural networks can learn the functional relationship between transmitted and reflected speckle patterns, enabling transmission control based solely on reflected light, a capability with important implications for in vivo applications. The integration of separable natural evolution strategies with multi-pixel encoded digital micromirror devices [176] has further accelerated wavefront optimization, achieving enhancement factors 16 times higher than conventional DMD-based methods. Neural wavefront shaping (NeuWS) proposed by Feng et al. [177] integrates maximum likelihood estimation, measurement modulation, and neural signal representations to reconstruct diffraction-limited images through strong static and dynamic scattering media without guidestars or controlled illumination, representing a significant advance in guidestar-free imaging.

Digital optical phase conjugation: Digital optical phase conjugation (DOPC) achieves focusing inside scattering media by time-reversing scattered wavefronts, corresponding to a physical inversion of the TM. Pioneering experimental advances established high-speed DOPC with millisecond-scale latencies [178] and full-polarization phase conjugation that doubles the focal contrast through thick biological tissues [179], creating a robust experimental framework upon which AI-driven optimization could build. It is worth noting that some optimization approaches for DOPC systems, such as the particle swarm algorithm employed by Cheng et al. [180], rely on conventional heuristic search rather than deep learning, but they illustrate the broader trend of computational intelligence in wavefront control. More recently, Ozcan and colleagues [181] demonstrated a diffractive wavefront processor optimized using deep learning to perform all-optical phase conjugation at the speed of light propagation without any digital computing, bridging traditional nonlinear optical phase conjugation with data-driven optimization.

5.2. Modal Coupling Systems

Multimode fibers represent a physically distinct class of scattering platforms where propagation is governed by modal mixing and dispersion rather than volumetric multiple scattering. The input-output relationship can likewise be described by a transmission matrix, which in this case takes the form of a high-dimensional mixing matrix acting on guided modes. Unlike the statistically random TMs of disordered media, multimode fiber TMs possess structured modal properties determined by fiber geometry, refractive index profile, and environmental conditions. This structural regularity makes multimode fiber TMs particularly amenable to neural network approximation.

5.2.1. Forward Modeling

Borhani et al. [159] showed that DNNs can learn the transmission matrix of kilometer-scale multimode fibers, reconstructing handwritten digits from intensity-only measurements. The study demonstrated that modal scrambling, though complex, remains learnable as a deterministic high-dimensional mixing process encoded in the TM.

Rahmani et al. [66] further demonstrated that CNNs can capture the nonlinear mapping between modulated inputs and output intensities in MMFs. Their work revealed that despite strong modal dispersion, the TM retains stable correlations that can be exploited by deep learning.

Compact network designs [168] confirmed that multimode fiber transmission matrices can be approximated efficiently. These findings support the view that MMF transmission matrices possess structured modal properties, distinct from the statistically distributed TMs of random multiple-scattering systems.

5.2.2. Inverse Reconstruction and Communication

For imaging applications, Caramazza et al. [160] demonstrated real-time transmission of natural scene images through MMFs by training a network to reconstruct images statistically, as shown in Figure 5d, effectively approximating the inverse transmission matrix.

Matthès et al. [182] addressed deformation sensitivity by learning transmission channels resilient to perturbations, revealing that certain modal subspaces of the TM remain stable under bending. This finding carries important practical implications, suggesting that robust MMF imaging systems can be constructed by selectively exploiting deformation-resilient modes.

Liu et al. [65] demonstrated ultra-high-speed image detection by exploiting modal dispersion within the transmission matrix to map two-dimensional spatial information into one-dimensional temporal pulse sequences, achieving frame rates of 15.4 Mfps with frame depths of 10,000 and demonstrating the potential for ultra-high-speed endoscopic imaging.

For optical communication, Pan et al. [183] introduced non-orthogonal optical multiplexing through MMFs using the SLRnet architecture, which learns the inverse mapping of the TM to simultaneously demultiplex multiple overlapping channels that share the same polarization, wavelength, and spatial region. Together, these works illustrate how neural networks approximate multimode fiber transmission matrices and their inverses in high-dimensional guided-wave systems.

5.3. Dynamic and Absorptive Scattering Systems

Dynamic and absorptive scattering systems introduce additional complexity beyond static multiple scattering, including strong absorption–scattering coupling, volumetric heterogeneity, and temporal variations due to environmental or physiological dynamics. Biological tissues represent a typical example of such systems, where the transmission matrix is not only high-dimensional and random but also lossy and time-dependent.

5.3.1. Forward Modeling

In dynamic scattering environments, neural networks provide a data-driven approach for modeling time-varying transmission behavior without requiring explicit physical characterization. Liu et al. [162] proposed a deep learning-based framework (DescatterNet) for real-time imaging through dynamic scattering media, including fog, turbid water, and biological tissues, as shown in Figure 5e. By training on paired scattered and reference images, the network learns a statistical mapping that compensates for distortions induced by inhomogeneous and temporally varying transmission matrices. The model further demonstrates generalization to previously unseen scenes and scattering conditions, indicating that neural networks can capture the underlying structure of nonstationary TMs.

Rivenson et al. [62] demonstrated deep learning microscopy, where a neural network transforms wide-field images into confocal-equivalent outputs by computationally compensating for distortions induced by the biological transmission matrix. In absorptive imaging modalities, such as optoacoustic tomography, Davoudi et al. [161] trained U-Net architectures to reconstruct high-resolution images from sparsely sampled data, effectively mitigating the degradation imposed by absorption and scattering processes encoded in the TM.

In absorptive measurement systems, deep learning has also been applied to reconstruct physical quantities from distorted imaging signals [163]. As shown in Figure 5f, neural networks can accurately predict laser energy absorptance from imaging data in laser processing systems. These studies collectively demonstrate that neural networks can approximate forward image formation processes even in lossy and dynamically evolving systems.

5.3.2. Inverse Imaging and Dynamic Compensation

Inverse problems in dynamic and absorptive scattering systems are particularly challenging due to temporal variations and loss mechanisms that continuously alter the transmission matrix. Learning-based approaches have shown strong capability in compensating for such nonstationary behavior. Sun et al. [184] extended speckle-based reconstruction methods to dynamic scattering media, demonstrating that neural networks can adapt to time-varying transmission matrices and recover object information beyond the limits of traditional correlation-based techniques.

Further developments in dynamic wave control have incorporated learning-based strategies into wavefront shaping frameworks. Guide-star-assisted wavefront shaping techniques [63] provide partial physical access to the transmission matrix, allowing neural networks to integrate measurement feedback with data-driven inversion strategies. In addition, fluorescence-based transmission matrix measurement techniques [185] enable noninvasive characterization of light propagation in biological tissues, providing complementary information that can enhance learning-based reconstruction. Together, these approaches highlight that neural networks function as effective approximators of time-varying and lossy transmission matrices, enabling inverse imaging, adaptive focusing, and dynamic compensation in some of the most challenging optical environments.

Complex scattering systems, including statistically disordered media, structured modal systems such as multimode fibers, and dynamic or absorptive scattering environments, share a common characteristic in that light propagation is governed by high-dimensional transmission matrices that are difficult to model or invert analytically. Although these platforms differ in their dominant physical mechanisms, ranging from statistical multiple scattering and structured modal coupling to absorptive and dynamic evolution, their input-output relationships can all be formulated in terms of transmission matrices. In this context, neural networks function as flexible approximators of high-dimensional transmission matrices and their inverses, enabling both forward prediction of system responses and inverse reconstruction or control without explicit transmission matrix measurement.

Across these systems, data-driven learning transforms complex wave propagation problems into tractable computational tasks. By implicitly capturing statistical correlations, modal structures, or time-dependent variations encoded in the transmission matrix, neural networks bridge measurement and control in regimes where traditional modeling becomes impractical. Future progress will depend on improving generalization under structural and environmental variations, incorporating physical constraints into network architectures, and extending learning-based approaches toward real-time adaptive operation in dynamic media. Together, these developments point toward a broader paradigm in photonics: learning effective transmission matrices directly from data to overcome the limitations of explicit analytical solutions.

6. Conclusions and Outlook

6.1. Comparative Analysis of AI Architectures

Sections 2–5 examined AI-driven design within each platform, where the choice of network was usually dictated by the specific physics and dimensionality of the problem. Viewed across platforms, the same small set of architectures reappears, and comparing them directly helps explain why a given method is favored in one setting and set aside in another. Table 1 summarizes seven architectures that recur throughout the literature and evaluates them against the dimensions most critical to that selection.

Table 1. Comparison of AI architectures.

Architecture	Typical Role	Data Requirement	Relative Training Cost	Inference Time	Scalability to Freedom Geometry	Training Robustness	Reference
FCNN	Forward; low-dim inverse	10^2–10^4	Low	~ms	Poor	High	[32]
CNN	Forward (image/freeform)	10^3–10^5	Moderate	~ms	Good	High	[86]
Tandem	Inverse (single solution)	10^3–10^4	Moderate (two networks)	~ms	Moderate	Moderate	[33]
GAN	Inverse (diverse, freeform)	10^4–10^5	High (adversarial)	~ms	Good	Low	[35]
cVAE	Inverse (diverse, uncertainty)	10^3–10^4	Moderate	~ms	Good	Moderate	[77]
RL	Sequential/discrete inverse	10^3–10^5 simulator calls	High (exploration)	~ms/step	Moderate	Low	[44]
PINN	Forward/inverse, data-scarce	10^1–10^3 (or data-free)	Moderate-High	~ms	Moderate	Moderate	[82,113]

What the table makes clear is that the architectures differ far less in practical performance than a lot of the literature might suggest. Every architecture in Table 1, once trained, returns a prediction in milliseconds, several orders of magnitude faster than the full-wave solver it replaces, so the acceleration highlighted in individual papers is in fact shared by all data-driven approaches and cannot by itself justify choosing one over another. Accuracy follows the same pattern, with reported errors falling to comparable levels across architectures whenever the training data are sufficient and the network is properly tuned, as the forward-modeling studies of earlier chapters repeatedly show.

The real distinction is therefore not how well or how fast they predict, but how they handle the structural difficulty that one target response can correspond to many distinct geometries. FCNNs and CNNs remain the natural choice for forward modeling and for inverse problems that are effectively single-valued, yet they falter once this one-to-many ambiguity appears, because the network then receives conflicting gradients during training. The architectures developed for this regime each resolve the conflict in their own way. Tandem networks score candidates in the response domain rather than the geometry domain, generative models such as GANs and cVAEs learn the full distribution of valid structures and so return diverse rather than averaged solutions, and reinforcement learning removes the need for a labeled dataset by treating design as a sequence of rewarded decisions. PINNs stand apart from all of these, lowering the data requirement by writing the governing equations directly into the loss.

Another recurring question in the field is how these data-driven methods compare with established gradient-based inverse design, particularly adjoint topology optimization. Table 2 places the two approaches side by side. The key distinction is not the speed for a single design, but how the computational cost is distributed across designs. Because adjoint optimization performs a forward and an adjoint simulation at every iteration and begins afresh for each new target, its total cost grows in proportion to the number of designs, whereas a trained network pays that cost only once, during dataset generation and training, and thereafter resolves each new target in a single forward pass. The practical implication is straightforward. Data-driven design pulls ahead wherever many designs, repeated targets, or real-time response are required, while adjoint optimization keeps the advantage for a small number of high-fidelity one-off targets.

Table 2. AI-driven inverse design versus adjoint topology optimization.

Criterion	Adjoint Topology Optimization	AI (Trained Network/Generative Model)
Cost model	Repeated in full for every new design	Concentrated in a one-time training phase, then reused across all designs
Simulations per design	~10^2–10^3 (one forward + one adjoint per iteration)	~0 after training (single ~ms forward pass)
Marginal cost of a new target	Full re-optimization	Near zero
Memory footprint	High (stores fields for gradient computation)	Modest (fixed network weights)
Convergence behavior	Local optimum near initialization	Samples the learned distribution; no optimality guarantee
Preferred regime	Few one-off, high-fidelity targets	Many designs, repeated targets, or real-time response

6.2. Critical Evaluation Across Platforms

Section 6.1 distinguished the architectures by their strengths. At the same time, they share a set of limitations that remain the same regardless of which network is chosen. Together, these limitations explain why most of the results reviewed here are still limited to simulation.

The most concrete of these is the reliance on large labeled datasets. Every supervised model depends on pairs of structures and their simulated responses, and generating such pairs is rarely cheap. A single full-wave simulation of a three-dimensional nanostructure can take hours, and the cost multiples with the dimensionality of the design space grows,

https://doi.org/10.3390/aimater1020005

so the data burden varies dramatically across platforms. Localized resonant nanostructures, which typically involve fewer than ten continuous parameters, can be handled with datasets on the order of 10^3 to 10^4 samples. By contrast, freeform unit cells and metasurface arrays demand far larger collections, and complex scattering systems pose an even greater challenge, because their transmission matrices usually must be measured rather than computed. This pattern is also visible in the data-hungry architectures of Table 1, the GANs and cVAEs in particular, which have been most often applied to lower-dimensional platforms.

This dependence on data directly leads to a related weakness, the tendency to overfit and to generalize poorly outside the training distribution. A network that interpolates accurately within its training range often fails when given a target outside it, and the failure is difficult to anticipate because the model gives no signal that it has left familiar ground. The risk is greatest where data are scarcest. High-Q photonic crystal cavities illustrate this sharply. The narrow resonances that determine their performance occupy only a tiny fraction of the design space, so a network trained on limited samples can easily miss them. Deterministic inverse models carry a related vulnerability, as a tandem network can be no more accurate than the frozen forward network at its core, so any bias in that surrogate propagates silently into every structure it generates.

Underlying both of these limitations is the hardest one to eliminate, which is that the models themselves are opaque. The geometric parameters of a metamaterial interact through electromagnetic coupling that a network distributes across millions of weights. There is no guarantee that any of these weights correspond to recognizable physical quantities, such as resonance modes or coupling strengths. For the designer, this lack of transparency has a sharp practical consequence. A black-box model cannot show whether a proposed structure respects constraints that were not included in the training data, nor can it indicate how far a novel target can be trusted before its predictions begin to degrade. This concern becomes critical once a design is meant for fabrication rather than illustration.

These limitations are not independent. Scarce data make overfitting more likely, overfitting is hard to detect without interpretable models, and opacity in turn hides how a design will behave once it moves beyond the simulator. That final step, from a converged simulation to a measured device, is where their combined impact is felt most significantly, and it is the focus of the next section.

6.3. Sim-to-Experiment Gap and Foundry-Level Constraints

Last section ended at the boundary between a converged simulation and a fabricated device. Crossing that boundary is where AI-driven design has so far been weakest. Experimental confirmation has been reported for optical information storage in nanostructures [70], for the band structure of photonic crystal slabs supporting bound states in the continuum [123], for record-Q photonic crystal cavities [146], and for imaging through multimode fibers [159], yet these remain isolated demonstrations rather than routine practice. The field still lacks an established closed-loop workflow in which measured data feed back to correct the network, so the reported accuracy of most models is an accuracy against simulation rather than against the physical world.

The gap between simulation and experiment has a common origin, though its severity varies by platforms. Networks are trained on idealized geometries, while fabrication introduces sidewall roughness, corner rounding, and variation in etch depth, none of which the model has seen. How much this mismatch matters depends on the structures. High-Q photonic crystal cavities represent the extreme case, since a displacement of only a few nanometers in a single air hole can lower the quality factor by orders of magnitude [138], turning a design that is optimal in simulation into a mediocre one once it is written into silicon. Complex scattering systems fail for a different reason. The medium they target changes over time, often faster than any fixed design can track [162], so the target medium on which the network was trained may no longer exist.

Another obstacle lies in the foundry design rules that any structure must satisfy before it can be fabricated. Neural networks typically output continuous geometric parameters, whereas lithographic processes demand a discrete grid, a minimum feature size fixed by the resolution limit, and a set of design rule checks that govern spacing, curvature, and enclosure. A structure that violates these rules cannot be manufactured, regardless of its simulated performance. Topology-optimized designs, which produce binary material distributions on a grid, fit naturally within this framework. In contrast, most generative models produce smooth, continuous geometries that must be binarized afterwards, and this step may cancel out the performance gains that the model was chosen for. Bridging this gap calls for design rules to be treated as part of the optimization objective, rather than as a filter applied after the fact.

Efforts to close this gap have so far remained partial. Augmenting the training set with random perturbations encourages a network to favor robust designs, but random noise is a poor substitute for real fabrication. Real processes introduce systematic biases such as proximity effects in lithography, loading effects in etching, and material-dependent non-uniformity in deposition, none of which symmetric random sampling can reproduce. Generative models that supply several valid candidates and transfer learning that adapts a model to altered conditions both help, yet neither addresses the core difficulty that fabrication error is process-specific and resists any general description. These shortcomings point to is not a single solution but a set of concrete algorithmic strategies.

6.4. Algorithmic Roadmaps for Grand Challenges

The limitations discussed in the previous sections are not all equally easy to overcome, but each now has at least one credible way forward. Instead of treating them as open problems, we pair them with the algorithmic strategies that aim to address them, grouped as data efficiency, interpretability, and experimental feasibility.

The data bottleneck has attracted the most mature set of solutions, two of which deserve a precise description because they directly reduce the amount of data required. The first strategy embeds the governing physics into the training objective. While a purely data-driven model minimizes only the mismatch against simulated labels, a physics-informed network adds a term that penalizes any violation of Maxwell's equations at a set of collocation points. For a frequency-domain field $\boldsymbol{E}$, the physics residual takes the form:

$$\mathcal{L}_{\text{physics}} = \frac{1}{N_c}\sum_{j=1}^{N_c}\left\|\nabla \times \nabla \times \boldsymbol{E}(\boldsymbol{r}_j) - \frac{\omega^2}{c^2}\varepsilon_r(\boldsymbol{r}_j)\boldsymbol{E}(\boldsymbol{r}_j)\right\|^2 \quad (6)$$

evaluated at N_c collocation points r_j that require no labels of their own. Because these points encode physical laws without the cost of additional simulations, the network can reach comparable accuracy with only a fraction of the labeled data. The weight λ in the Combined objective $\mathcal{L} = \mathcal{L}_{\text{data}} + \lambda\mathcal{L}_{\text{physics}}$ of Equation (5) controls how strongly the physics is enforced. Physics-driven training along these lines has already been demonstrated for metasurface design [82,113]. The second response makes data collection adaptive. Instead of sampling the design space uniformly, Bayesian active learning queries the simulator only where the current model is least certain, selecting the next structure as:

$$\mathbf{x}^* = \underset{\mathbf{x}}{\text{argmax}}\,\sigma^2(\mathbf{x}) \quad (7)$$

where $\sigma^2(\mathbf{x})$ is the predictive variance of the surrogate, estimated from a model ensemble or a Bayesian network. The chosen structure is simulated, added to the training set, and the model retrained, so that each new simulation is spent where it most reduces uncertainty. Although this strategy remains uncommon in metamaterial design, it is indicated by reinforcement-learning schemes that query a solver dynamically during training rather than learning from a fixed dataset [124].

Interpretability is harder to address directly, because it demands not a smaller dataset but an understanding of what the model has learned. Even so, several concrete tools now exist. Feature attribution methods quantify the contribution of each geometric parameter to a given spectral feature. This makes it possible to identify which dimension of a unit cell controls a particular resonance, rather than leaving that relationship buried in the weights. Attention mechanisms serve a similar role inside the network, revealing which parts of an input geometry the model weights most heavily when making a prediction, though it should be noted that these attention weights reflect correlation, not causation. The most ambitious approach is symbolic regression, which searches for a compact, closed-form expression that reproduces the learned mapping, effectively turning the network from a predictor into a candidate physical law that can be tested against established electromagnetic theory. None of these methods achieves full transparency, but together they shift interpretability from a distant goal toward a set of practical diagnostic tools.

Experimental feasibility is best approached by writing the constraints that caused earlier designs to fail directly into the objective function. A process-aware loss works by adding a penalty for unmanufacturable features to the performance term:

$$\mathcal{L} = \mathcal{L}_{\text{performance}} + \lambda_{\text{fab}}\mathcal{L}_{\text{fab}} \tag{8}$$

where the fabrication loss $\mathcal{L}_{\text{fab}}$ grows whenever a design contains features below the resolution limit or spacings smaller than the minimum allowed. In this way, the network is steered toward structures that satisfy the design rules from the start rather than after the fact. This penalty shares the same form as the physics-informed objective discussed above, differing only in what the added term encodes. It embeds the rules of a fabrication process instead of the laws of electromagnetism. Two further elements help close the loop between simulation and the laboratory. A digital twin, a differentiable model of the fabrication process fitted to measured data, allows systematic biases such as proximity and loading effects to be anticipated during design rather than discovered afterwards. Domain adaptation then aligns the statistics of simulated and measured responses. As a result, a model trained mostly in simulation can be corrected with a small number of fabricated samples instead of an entirely new dataset.

These roadmaps share a common theme. In each case, the approach works by adding an extra term or an adaptive rule on top of the basic learning objective, whether the goal is to enforce physical laws, to reveal what the model has learned, or to respect the limits of a fabrication process. What remains harder to judge is how well any of these solutions will hold up as models and design spaces continue to scale.

6.5. Scaling Laws, Hybrid Physics-AI, and Adaptive Real-Time Systems

The roadmaps in last section assume that models remain roughly at their current size. However, recent experience elsewhere in machine learning suggests they will not. In language and vision, performance has been found to improve in a predictable, power-law manner as datasets, parameter counts, and training compute grow together, and these scaling laws have become the central driver of progress. Whether the same regularity applies to nanophotonics is now an open question. In most fields, the data that fuel scaling can be gathered at little cost. By contrast, every training example requires a full-wave simulation in metamaterial design. As a result, the volume of training data, which is the dimension we would most like to scale, turns out to be the most expensive one. This difference reshapes the trade-off rather than removing it. Progress in this field will depend less on raw data volume and more on lowering the data cost of each performance improvement. Physics-informed training extracts more information from every sample, while a model shared across platforms distributes the simulation cost over the whole community, so it does not need to be repeated for each new system.

Early signs of this shift are already visible. Foundation models trained on broad collections of structures, such as OptoGPT for multilayer films [130] and the Bayesian transformer MetaFO [186], show that a single model can serve many design problems once it has captured enough of the underlying regularities. Representation-learning methods that compress the design space into compact latent variables point in the same direction, improving both generalization and data efficiency [187]. The common trend is toward models that are trained once for the entire field and then reused, rather than rebuilt for each new platform.

A different kind of scaling pressure appears where reconfigurable platforms must respond continuously rather than just once. A metasurface that steers its beam in real time, or a cloak that tracks a moving target, cannot stop to retrain. Here the critical limit is no longer the size of the dataset, but the time it takes to run a single inference. Studies on real-time data-driven beam steering [101] and on reinforcement-learning control of focusing through obstacles [106] have shown that closed-loop operation at the required speed is possible. Yet these systems still rely on models that were trained in advance on the expected range of conditions. The frontier here is online adaptation, where a lightweight model deployed on the device updates itself from live measurements. This also raises a hardware challenge, because each inference must be completed within the millisecond timescale that reconfigurable operation demands.

6.6. Outlook

Looking further ahead, it is entirely possible that design will no longer be a matter of humans handing a model one problem at a time. Kim et al. demonstrated that large language models can perform inverse design of multilayer thin films through in-context learning and metasurfaces through fine-tuning with text-based structural representations, enabling nanophotonic design accessible to a wider audience without domain-specific expertise [188]. This trajectory is further exemplified by the metamaterial agent of Hu et al., which is endowed with reasoning and cognitive capabilities that enable the autonomous planning and execution of diverse electromagnetic manipulation tasks [189], pointing toward a future in which metamaterial systems transition from passive design objects to autonomous intelligent platforms.

Combined with the foundation models discussed in Section 6.5, such agents point toward metamaterial systems that move beyond being passive design targets. Instead, these systems become platforms capable of specifying, simulating, and refining their own structures. A closely related direction, still largely unexplored, is the integration of different length scales and physical domains. Real-world metamaterial devices involve coupled phenomena across multiple scales, from nanoscale resonances to macroscale device integration, and across multiple physical domains including electromagnetic, thermal, and mechanical responses. Developing hierarchical neural network architectures that bridge these scales and couple these physical domains would enable truly system-level optimization that accounts for the full complexity of practical devices.

In summary, AI-driven optical metamaterial design has achieved remarkable progress in accelerating forward prediction and enabling inverse design. Yet the limitations examined in this chapter, including dependence on costly data, the lack of transparency of the models, and the gap between simulation and fabrication, remain the main barriers to its use as a reliable engineering tool. Importantly, these challenges are deeply connected. Progress on any one of them often requires progress on the others, so the advance of the field will require close collaboration among the machine learning, electromagnetics, and nanofabrication communities rather than through any single algorithmic breakthrough.

Funding: This work is supported by National Natural Science Foundation of China (12474293, 12174188, 12404364, 12374293), Natural Science Foundation of Jiangsu Province (BK20233001, BK20240575), and the Postdoctoral Fellowship Program of CPSF (GZC20252238).

Data Availability Statement: No new data were created or analyzed in this study. Data sharing is not applicable to this article.

Conflicts of Interest: The authors declare no conflicts of interest.

References

1. Smith, D.R.; Padilla, W.J.; Vier, D.C.; Nemat-Nasser, S.C.; Schultz, S. Composite Medium with Simultaneously Negative Permeability and Permittivity. *Phys. Rev. Lett.* **2000**, *84*, 4184–4187. [CrossRef]
2. Veselago, V.G. Electrodynamics of Substances with Simultaneously Negative Values of ϵ and μ. *Sov. Phys. Uspekhi-Ussr* **1968**, *10*, 509–514. [CrossRef]
3. Pendry, J.B. Negative Refraction Makes a Perfect Lens. *Phys. Rev. Lett.* **2000**, *85*, 3966–3969. [CrossRef] [PubMed]
4. Shelby, R.A.; Smith, D.R.; Schultz, S. Experimental Verification of a Negative Index of Refraction. *Science* **2001**, *292*, 77–79. [CrossRef] [PubMed]
5. Smith, D.R.; Pendry, J.B.; Wiltshire, M.C.K. Metamaterials and Negative Refractive Index. *Science* **2004**, *305*, 788–792. [CrossRef] [PubMed]
6. Zheludev, N.I.; Kivshar, Y.S. From metamaterials to metadevices. *Nat. Mater.* **2012**, *11*, 917–924. [CrossRef] [PubMed]
7. Pendry, J.B.; Schurig, D.; Smith, D.R. Controlling Electromagnetic Fields. *Science* **2006**, *312*, 1780–1782. [CrossRef] [PubMed]
8. Schurig, D.; Mock, J.J.; Justice, B.J.; Cummer, S.A.; Pendry, J.B.; Starr, A.F.; Smith, D.R. Metamaterial Electromagnetic Cloak at Microwave Frequencies. *Science* **2006**, *314*, 977–980. [CrossRef] [PubMed]
9. Leonhardt, U. Optical Conformal Mapping. *Science* **2006**, *312*, 1777–1780. [CrossRef] [PubMed]
10. Fang, N.; Lee, H.; Sun, C.; Zhang, X. Sub-Diffraction-Limited Optical Imaging with a Silver Superlens. *Science* **2005**, *308*, 534–537. [CrossRef] [PubMed]
11. Landy, N.I.; Sajuyigbe, S.; Mock, J.J.; Smith, D.R.; Padilla, W.J. Perfect Metamaterial Absorber. *Phys. Rev. Lett.* **2008**, *100*, 207402. [CrossRef] [PubMed]
12. Lu, L.; Joannopoulos, J.D.; Soljacic, M. Topological photonics. *Nat. Photonics* **2014**, *8*, 821–829. [CrossRef]
13. Yu, N.; Genevet, P.; Kats, M.A.; Aieta, F.; Tetienne, J.-P.; Capasso, F.; Gaburro, Z. Light Propagation with Phase Discontinuities: Generalized Laws of Reflection and Refraction. *Science* **2011**, *334*, 333–337. [CrossRef] [PubMed]
14. Tittl, A.; Leitis, A.; Liu, M.; Yesilkoy, F.; Choi, D.-Y.; Neshev, D.N.; Kivshar, Y.S.; Altug, H. Imaging-based molecular barcoding with pixelated dielectric metasurfaces. *Science* **2018**, *360*, 1105–1109. [CrossRef] [PubMed]
15. Raman, A.P.; Abou Anoma, M.; Zhu, L.X.; Rephaeli, E.; Fan, S.H. Passive radiative cooling below ambient air temperature under direct sunlight. *Nature* **2014**, *515*, 540–544. [CrossRef] [PubMed]
16. Piccinotti, D.; MacDonald, K.F.; A Gregory, S.; Youngs, I.; Zheludev, N.I. Artificial intelligence for photonics and photonic materials. *Rep. Prog. Phys.* **2021**, *84*, 012401. [CrossRef] [PubMed]
17. Deng, Y.; Ren, S.; Fan, K.; Malof, J.M.; Padilla, W.J. Neural-adjoint method for the inverse design of all-dielectric metasurfaces. *Opt. Express* **2021**, *29*, 7526–7534. [CrossRef] [PubMed]
18. Molesky, S.; Lin, Z.; Piggott, A.Y.; Jin, W.L.; Vuckovic, J.; Rodriguez, A.W. Inverse design in nanophotonics. *Nat. Photonics* **2018**, *12*, 659–670. [CrossRef]
19. Jensen, J.S.; Sigmund, O. Topology optimization for nano-photonics. *Laser Photonics Rev.* **2011**, *5*, 308–321. [CrossRef]
20. Vapnik, V.N. *The Nature of Statistical Learning Theory*; Springer: New York, NY, USA, 1995.
21. LeCun, Y.; Bengio, Y.; Hinton, G. Deep learning. *Nature* **2015**, *521*, 436–444. [CrossRef] [PubMed]
22. Krizhevsky, A.; Sutskever, I.; Hinton, G.E. ImageNet classification with deep convolutional neural networks. *Commun. ACM* **2017**, *60*, 84–90. [CrossRef]

23. Silver, D.; Huang, A.; Maddison, C.J.; Guez, A.; Sifre, L.; van den Driessche, G.; Schrittwieser, J.; Antonoglou, I.; Panneershelvam, V.; Lanctot, M.; et al. Mastering the game of Go with deep neural networks and tree search. *Nature* **2016**, *529*, 484–489. [CrossRef] [PubMed]
24. Jumper, J.; Evans, R.; Pritzel, A.; Green, T.; Figurnov, M.; Ronneberger, O.; Tunyasuvunakool, K.; Bates, R.; Žídek, A.; Potapenko, A.; et al. Highly accurate protein structure prediction with AlphaFold. *Nature* **2021**, *596*, 583–589. [CrossRef] [PubMed]
25. Goodfellow, I.J.; Pouget-Abadie, J.; Mirza, M.; Xu, B.; Warde-Farley, D.; Ozair, S.; Courville, A.; Bengio, Y. Generative Adversarial Nets. In Proceedings of the 28th Conference on Neural Information Processing Systems (NIPS), Montreal, QC, Canada, 8–13 December 2014; pp. 2672–2680.
26. Vaswani, A.; Shazeer, N.; Parmar, N.; Uszkoreit, J.; Jones, L.; Gomez, A.N.; Kaiser, L.; Polosukhin, I. Attention Is All You Need. In Proceedings of the 31st Annual Conference on Neural Information Processing Systems (NIPS), Long Beach, CA, USA, 4–9 December 2017.
27. Butler, K.T.; Davies, D.W.; Cartwright, H.; Isayev, O.; Walsh, A. Machine learning for molecular and materials science. *Nature* **2018**, *559*, 547–555. [CrossRef] [PubMed]
28. Khatib, O.; Ren, S.; Malof, J.; Padilla, W.J. Deep Learning the Electromagnetic Properties of Metamaterials—A Comprehensive Review. *Adv. Funct. Mater.* **2021**, *31*, 2101748. [CrossRef]
29. Piggott, A.Y.; Lu, J.; Lagoudakis, K.G.; Petykiewicz, J.; Babinec, T.M.; Vuckovic, J. Inverse design and demonstration of a compact and broadband on-chip wavelength demultiplexer. *Nat. Photonics* **2015**, *9*, 374–377. [CrossRef]
30. Weile, D.S.; Michielssen, E. Genetic algorithm optimization applied to electromagnetics: A review. *IEEE Trans. Antennas Propag.* **1997**, *45*, 343–353. [CrossRef]
31. Forestiere, C.; Donelli, M.; Walsh, G.F.; Zeni, E.; Miano, G.; Dal Negro, L. Particle-swarm optimization of broadband nanoplasmonic arrays. *Opt. Lett.* **2010**, *35*, 133–135. [CrossRef] [PubMed]
32. Peurifoy, J.; Shen, Y.; Jing, L.; Yang, Y.; Cano-Renteria, F.; DeLacy, B.G.; Joannopoulos, J.D.; Tegmark, M.; Soljačić, M. Nanophotonic particle simulation and inverse design using artificial neural networks. *Sci. Adv.* **2018**, *4*, eaar4206. [CrossRef] [PubMed]
33. Liu, D.; Tan, Y.; Khoram, E.; Yu, Z. Training Deep Neural Networks for the Inverse Design of Nanophotonic Structures. *ACS Photonics* **2018**, *5*, 1365–1369. [CrossRef]
34. Ma, W.; Cheng, F.; Liu, Y. Deep-Learning-Enabled On-Demand Design of Chiral Metamaterials. *ACS Nano* **2018**, *12*, 6326–6334. [CrossRef] [PubMed]
35. Liu, Z.; Zhu, D.; Rodrigues, S.P.; Lee, K.-T.; Cai, W. Generative Model for the Inverse Design of Metasurfaces. *Nano Lett.* **2018**, *18*, 6570–6576. [CrossRef] [PubMed]
36. Ma, W.; Cheng, F.; Xu, Y.; Wen, Q.; Liu, Y. Probabilistic Representation and Inverse Design of Metamaterials Based on a Deep Generative Model with Semi-Supervised Learning Strategy. *Adv. Mater.* **2019**, *31*, e1901111. [CrossRef] [PubMed]
37. Sajedian, I.; Lee, H.; Rho, J. Double-deep Q-learning to increase the efficiency of metasurface holograms. *Sci. Rep.* **2019**, *9*, 10899. [CrossRef] [PubMed]
38. Qian, C.; Kaminer, I.; Chen, H. A guidance to intelligent metamaterials and metamaterials intelligence. *Nat. Commun.* **2025**, *16*, 1154. [CrossRef] [PubMed]
39. Tezsezen, E.; Yigci, D.; Ahmadpour, A.; Tasoglu, S. AI-Based Metamaterial Design. *ACS Appl. Mater. Interfaces* **2024**, *16*, 29547–29569. [CrossRef] [PubMed]
40. An, S.; Fowler, C.; Zheng, B.; Shalaginov, M.Y.; Tang, H.; Li, H.; Zhou, L.; Ding, J.; Agarwal, A.M.; Rivero-Baleine, C.; et al. A Deep Learning Approach for Objective-Driven All-Dielectric Metasurface Design. *ACS Photonics* **2019**, *6*, 3196–3207. [CrossRef]
41. Gao, L.; Li, X.; Liu, D.; Wang, L.; Yu, Z. A Bidirectional Deep Neural Network for Accurate Silicon Color Design. *Adv. Mater.* **2019**, *31*, e1905467. [CrossRef] [PubMed]
42. Jiang, J.; Sell, D.; Hoyer, S.; Hickey, J.; Yang, J.; Fan, J.A. Free-Form Diffractive Metagrating Design Based on Generative Adversarial Networks. *ACS Nano* **2019**, *13*, 8872–8878. [CrossRef] [PubMed]
43. Zheng, L.; Karapiperis, K.; Kumar, S.; Kochmann, D.M. Unifying the design space and optimizing linear and nonlinear truss metamaterials by generative modeling. *Nat. Commun.* **2023**, *14*, 7563. [CrossRef] [PubMed]
44. Sajedian, I.; Badloe, T.; Rho, J. Optimisation of colour generation from dielectric nanostructures using reinforcement learning. *Opt. Express* **2019**, *27*, 5874–5883. [CrossRef] [PubMed]
45. Hughes, T.W.; Minkov, M.; Williamson, I.A.D.; Fan, S. Adjoint Method and Inverse Design for Nonlinear Nanophotonic Devices. *ACS Photonics* **2018**, *5*, 4781–4787. [CrossRef]
46. Maier, S.A. *Plasmonics: Fundamentals and Applications*; Springer: New York, NY, USA, 2007; pp. 1–223.
47. Kuznetsov, A.I.; Miroshnichenko, A.E.; Brongersma, M.L.; Kivshar, Y.S.; Luk'yanchuk, B. Optically resonant dielectric nanostructures. *Science* **2016**, *354*, aag2472. [CrossRef] [PubMed]
48. Khorasaninejad, M.; Chen, W.T.; Devlin, R.C.; Oh, J.; Zhu, A.Y.; Capasso, F. Metalenses at visible wavelengths: Diffraction-limited focusing and subwavelength resolution imaging. *Science* **2016**, *352*, 1190–1194. [CrossRef] [PubMed]

49. Zheng, G.X.; Mühlenbernd, H.; Kenney, M.; Li, G.X.; Zentgraf, T.; Zhang, S. Metasurface holograms reaching 80% efficiency. *Nat. Nanotechnol.* **2015**, *10*, 308–312. [CrossRef] [PubMed]
50. Huang, L.; Chen, X.; Mühlenbernd, H.; Zhang, H.; Chen, S.; Bai, B.; Tan, Q.; Jin, G.; Cheah, K.-W.; Qiu, C.-W.; et al. Three-dimensional optical holography using a plasmonic metasurface. *Nat. Commun.* **2013**, *4*, 2808. [CrossRef]
51. Grady, N.K.; Heyes, J.E.; Chowdhury, D.R.; Zeng, Y.; Reiten, M.T.; Azad, A.K.; Taylor, A.J.; Dalvit, D.A.R.; Chen, H.-T. Terahertz Metamaterials for Linear Polarization Conversion and Anomalous Refraction. *Science* **2013**, *340*, 1304–1307. [CrossRef] [PubMed]
52. John, S. Strong localization of photons in certain disordered dielectric superlattices. *Phys. Rev. Lett.* **1987**, *58*, 2486–2489. [CrossRef] [PubMed]
53. Yablonovitch, E. Inhibited Spontaneous Emission in Solid-State Physics and Electronics. *Phys. Rev. Lett.* **1987**, *58*, 2059–2062. [CrossRef] [PubMed]
54. Joannopoulos, J.D.; Johnson, S.G.; Winn, J.N.; Meade, R.D. *Photonic Crystals: Molding the Flow of Light*, 2nd ed.; Princeton University Press: Princeton, NJ, USA, 2008.
55. Ferreira, A.d.S.; Malheiros-Silveira, G.N.; Hernández-Figueroa, H.E. Computing Optical Properties of Photonic Crystals by Using Multilayer Perceptron and Extreme Learning Machine. *J. Light. Technol.* **2018**, *36*, 4066–4073. [CrossRef]
56. Pilozzi, L.; Farrelly, F.A.; Marcucci, G.; Conti, C. Machine learning inverse problem for topological photonics. *Commun. Phys.* **2018**, *1*, 57. [CrossRef]
57. Chen, J.; Hao, R.; Nasidi, I.; Zhang, H.; Wang, X.; Jin, S. Deep Learning-Based Modelling of Complex Photonic Crystal Slow Light Waveguides. *IEEE J. Sel. Top. Quantum Electron.* **2023**, *29*, 6101506. [CrossRef]
58. Rotter, S.; Gigan, S. Light fields in complex media: Mesoscopic scattering meets wave control. *Rev. Mod. Phys.* **2017**, *89*, 015005. [CrossRef]
59. Mosk, A.P.; Lagendijk, A.; Lerosey, G.; Fink, M. Controlling waves in space and time for imaging and focusing in complex media. *Nat. Photonics* **2012**, *6*, 283–292. [CrossRef]
60. Popoff, S.M.; Lerosey, G.; Carminati, R.; Fink, M.; Boccara, A.C.; Gigan, S. Measuring the Transmission Matrix in Optics: An Approach to the Study and Control of Light Propagation in Disordered Media. *Phys. Rev. Lett.* **2010**, *104*, 100601. [CrossRef] [PubMed]
61. Li, Y.; Xue, Y.; Tian, L. Deep speckle correlation: A deep learning approach toward scalable imaging through scattering media. *Optica* **2018**, *5*, 1181–1190. [CrossRef]
62. Rivenson, Y.; Göröcs, Z.; Günaydin, H.; Zhang, Y.; Wang, H.; Ozcan, A. Deep learning microscopy. *Optica* **2017**, *4*, 1437–1443. [CrossRef]
63. Horstmeyer, R.; Ruan, H.W.; Yang, C.H. Guidestar-assisted wavefront-shaping methods for focusing light into biological tissue. *Nat. Photonics* **2015**, *9*, 563–571. [CrossRef] [PubMed]
64. Luo, Y.; Yan, S.; Li, H.; Lai, P.; Zheng, Y. Towards smart optical focusing: Deep learning-empowered dynamic wavefront shaping through nonstationary scattering media. *Photon. Res.* **2021**, *9*, B262–B278. [CrossRef]
65. Liu, Z.; Wang, L.; Meng, Y.; He, T.; He, S.; Yang, Y.; Wang, L.; Tian, J.; Li, D.; Yan, P.; et al. All-fiber high-speed image detection enabled by deep learning. *Nat. Commun.* **2022**, *13*, 1433. [CrossRef] [PubMed]
66. Rahmani, B.; Loterie, D.; Konstantinou, G.; Psaltis, D.; Moser, C. Multimode optical fiber transmission with a deep learning network. *Light Sci. Appl.* **2018**, *7*, 69. [CrossRef] [PubMed]
67. Ma, W.; Liu, Z.; Kudyshev, Z.A.; Boltasseva, A.; Cai, W.; Liu, Y. Deep learning for the design of photonic structures. *Nat. Photonics* **2021**, *15*, 77–90. [CrossRef]
68. Malkiel, I.; Mrejen, M.; Nagler, A.; Arieli, U.; Wolf, L.; Suchowski, H. Plasmonic nanostructure design and characterization via Deep Learning. *Light Sci. Appl.* **2018**, *7*, 60. [CrossRef] [PubMed]
69. He, J.; He, C.; Zheng, C.; Wang, Q.; Ye, J. Plasmonic nanoparticle simulations and inverse design using machine learning. *Nanoscale* **2019**, *11*, 17444–17459. [CrossRef] [PubMed]
70. Wiecha, P.R.; Lecestre, A.; Mallet, N.; Larrieu, G. Pushing the limits of optical information storage using deep learning. *Nat. Nanotechnol.* **2019**, *14*, 237–244. [CrossRef] [PubMed]
71. Wiecha, P.R.; Muskens, O.L. Deep Learning Meets Nanophotonics: A Generalized Accurate Predictor for Near Fields and Far Fields of Arbitrary 3D Nanostructures. *Nano Lett.* **2020**, *20*, 329–338. [CrossRef] [PubMed]
72. Wu, Q.; Li, X.; Wang, W.; Dong, Q.; Xiao, Y.; Cao, X.; Wang, L.; Gao, L. Comparison of Different Neural Network Architectures for Plasmonic Inverse Design. *ACS Omega* **2021**, *6*, 23076–23082. [CrossRef] [PubMed]
73. So, S.; Mun, J.; Rho, J. Simultaneous Inverse Design of Materials and Structures via Deep Learning: Demonstration of Dipole Resonance Engineering Using Core–Shell Nanoparticles. *ACS Appl. Mater. Interfaces* **2019**, *11*, 24264–24268. [CrossRef] [PubMed]
74. Guo, J.; Zhang, Y.; Huang, M.; Xu, Y.; Fan, H.; Liu, W.; Lai, Y.; Gao, L.; Luo, J. Electromagnetically large cylinders with duality symmetry by hybrid neural networks. *Opt. Laser Technol.* **2024**, *168*, 109935. [CrossRef]
75. Adibnia, E.; Ghadrdan, M.; Mansouri-Birjandi, M.A. Nanophotonic structure inverse design for switching application using deep learning. *Sci. Rep.* **2024**, *14*, 21094. [CrossRef] [PubMed]

76. Adibnia, E.; Mansouri-Birjandi, M.A.; Ghadrdan, M.; Jafari, P. A deep learning method for empirical spectral prediction and inverse design of all-optical nonlinear plasmonic ring resonator switches. *Sci. Rep.* **2024**, *14*, 5787. [CrossRef] [PubMed]
77. Rahman, T.; Tahmid, A.; Arman, S.E.; Ahmed, T.; Rakhy, Z.T.; Das, H.; Rahman, M.; Azad, A.K.; Wahadoszamen, M.; Habib, A. Leveraging generative neural networks for accurate, diverse, and robust nanoparticle design. *Nanoscale Adv.* **2025**, *7*, 634–642. [CrossRef] [PubMed]
78. Hegde, R.S. Photonics Inverse Design: Pairing Deep Neural Networks With Evolutionary Algorithms. *IEEE J. Sel. Top. Quantum Electron.* **2020**, *26*, 7700908. [CrossRef]
79. Sun, S.; He, Q.; Hao, J.; Xiao, S.; Zhou, L. Electromagnetic metasurfaces: Physics and applications. *Adv. Opt. Photon.* **2019**, *11*, 380–479. [CrossRef]
80. An, S.; Zheng, B.; Shalaginov, M.Y.; Tang, H.; Li, H.; Zhou, L.; Ding, J.; Agarwal, A.M.; Rivero-Baleine, C.; Kang, M.; et al. Deep learning modeling approach for metasurfaces with high degrees of freedom. *Opt. Express* **2020**, *28*, 31932–31942. [CrossRef] [PubMed]
81. Pestourie, R.; Mroueh, Y.; Nguyen, T.V.; Das, P.; Johnson, S.G. Active learning of deep surrogates for PDEs: Application to metasurface design. *npj Comput. Mater.* **2020**, *6*, 164. [CrossRef]
82. Chen, W.-Q.; Zhang, D.-S.; Long, S.-Y.; Liu, Z.-Z.; Xiao, J.-J. Nearly dispersionless multicolor metasurface beam deflector for near eye display designed by a physics-driven deep neural network. *Appl. Opt.* **2021**, *60*, 3947–3953. [CrossRef] [PubMed]
83. Zhu, R.; Qiu, T.; Wang, J.; Sui, S.; Hao, C.; Liu, T.; Li, Y.; Feng, M.; Zhang, A.; Qiu, C.-W.; et al. Phase-to-pattern inverse design paradigm for fast realization of functional metasurfaces via transfer learning. *Nat. Commun.* **2021**, *12*, 2974. [CrossRef] [PubMed]
84. Fan, Z.; Qian, C.; Jia, Y.; Chen, M.; Zhang, J.; Cui, X.; Li, E.-P.; Zheng, B.; Cai, T.; Chen, H. Transfer-Learning-Assisted Inverse Metasurface Design for 30% Data Savings. *Phys. Rev. Appl.* **2022**, *18*, 024022. [CrossRef]
85. Inampudi, S.; Mosallaei, H. Neural network based design of metagratings. *Appl. Phys. Lett.* **2018**, *112*, 241102. [CrossRef]
86. Sajedian, I.; Kim, J.; Rho, J. Finding the optical properties of plasmonic structures by image processing using a combination of convolutional neural networks and recurrent neural networks. *Microsyst. Nanoeng.* **2019**, *5*, 27. [CrossRef] [PubMed]
87. Pillai, P.; Pal, P.; Chacko, R.; Jain, D.; Rai, B. Leveraging long short-term memory (LSTM)-based neural networks for modeling structure–property relationships of metamaterials from electromagnetic responses. *Sci. Rep.* **2021**, *11*, 18629. [CrossRef] [PubMed]
88. So, S.; Rho, J. Designing nanophotonic structures using conditional deep convolutional generative adversarial networks. *Nanophotonics* **2019**, *8*, 1255–1261. [CrossRef]
89. Qiu, T.; Shi, X.; Wang, J.; Li, Y.; Qu, S.; Cheng, Q.; Cui, T.; Sui, S. Deep Learning: A Rapid and Efficient Route to Automatic Metasurface Design. *Adv. Sci.* **2019**, *6*, 1900128. [CrossRef] [PubMed]
90. Nadell, C.C.; Huang, B.; Malof, J.M.; Padilla, W.J. Deep learning for accelerated all-dielectric metasurface design. *Opt. Express* **2019**, *27*, 27523–27535. [CrossRef] [PubMed]
91. Yang, B.; Ma, D.; Liu, W.; Choi, D.-Y.; Li, Z.; Cheng, H.; Tian, J.; Chen, S. Deep-learning-based colorimetric polarization-angle detection with metasurfaces. *Optica* **2022**, *9*, 217–220. [CrossRef]
92. Liu, Z.; Zhu, D.; Lee, K.-T.; Kim, A.S.; Raju, L.; Cai, W. Compounding Meta-Atoms into Metamolecules with Hybrid Artificial Intelligence Techniques. *Adv. Mater.* **2020**, *32*, 1904790. [CrossRef] [PubMed]
93. Zhu, R.; Han, Y.; Jia, Y.; Sui, S.; Liu, T.; Chu, Z.; Sun, H.; Jiang, J.; Qu, S.; Wang, J. Multifunctional Metasurface Design via Physics-Simplified Machine Learning. *Int. J. Intell. Syst.* **2025**, *2025*, 1492020. [CrossRef]
94. Fan, Z.; Qian, C.; Jia, Y.; Feng, Y.; Qian, H.; Li, E.-P.; Fleury, R.; Chen, H. Holographic multiplexing metasurface with twisted diffractive neural network. *Nat. Commun.* **2024**, *15*, 9416. [CrossRef] [PubMed]
95. Huang, Y.; Liu, X.; Liu, M.; Chen, J.; Du, W.; Liu, Z. Deep learning-based inverse design of multi-functional metasurface absorbers. *Opt. Lett.* **2024**, *49*, 2733–2736. [CrossRef] [PubMed]
96. Qian, C.; Zheng, B.; Shen, Y.C.; Jing, L.; Li, E.P.; Shen, L.; Chen, H.S. Deep-learning-enabled self-adaptive microwave cloak without human intervention. *Nat. Photonics* **2020**, *14*, 383–390. [CrossRef]
97. Wang, Z.; Qian, C.; Lin, P.; Zheng, B.; Kim, G.; Noh, J.; Li, E.; Rho, J.; Chen, H. 3D Intelligent Cloaked Vehicle Equipped with Thousand-Level Reconfigurable Full-Polarization Metasurfaces. *Adv. Mater.* **2024**, *36*, 2400797. [CrossRef] [PubMed]
98. Qian, C.; Jia, Y.; Wang, Z.; Chen, J.; Lin, P.; Zhu, X.; Li, E.; Chen, H. Autonomous aeroamphibious invisibility cloak with stochastic-evolution learning. *Adv. Photonics* **2024**, *6*, 016001. [CrossRef]
99. Fan, Z.; Qian, C.; Jia, Y.; Wang, Z.; Ding, Y.; Wang, D.; Tian, L.; Li, E.; Cai, T.; Zheng, B.; et al. Homeostatic neuro-metasurfaces for dynamic wireless channel management. *Sci. Adv.* **2022**, *8*, eabn7905. [CrossRef] [PubMed]
100. Li, W.; Ma, Q.; Liu, C.; Zhang, Y.; Wu, X.; Wang, J.; Gao, S.; Qiu, T.; Liu, T.; Xiao, Q.; et al. Intelligent metasurface system for automatic tracking of moving targets and wireless communications based on computer vision. *Nat. Commun.* **2023**, *14*, 989. [CrossRef] [PubMed]
101. Wen, E.; Yang, X.; Sievenpiper, D.F. Real-data-driven real-time reconfigurable microwave reflective surface. *Nat. Commun.* **2023**, *14*, 7736. [CrossRef] [PubMed]

102. Jia, Y.; Qian, C.; Fan, Z.; Cai, T.; Li, E.-P.; Chen, H. A knowledge-inherited learning for intelligent metasurface design and assembly. *Light Sci. Appl.* **2023**, *12*, 82. [CrossRef] [PubMed]
103. Jia, Y.; Fan, Z.; Qian, C.; del Hougne, P.; Chen, H. Dynamic Inverse Design of Broadband Metasurfaces with Synthetical Neural Networks. *Laser Photonics Rev.* **2024**, *18*, 2400063. [CrossRef]
104. Li, L.; Ruan, H.; Liu, C.; Li, Y.; Shuang, Y.; Alù, A.; Qiu, C.-W.; Cui, T.J. Machine-learning reprogrammable metasurface imager. *Nat. Commun.* **2019**, *10*, 1082. [CrossRef] [PubMed]
105. Lu, H.; Zhao, J.; Zheng, B.; Qian, C.; Cai, T.; Li, E.; Chen, H. Eye accommodation-inspired neuro-metasurface focusing. *Nat. Commun.* **2023**, *14*, 3301. [CrossRef] [PubMed]
106. Lu, H.; Zhu, R.; Wang, C.; Hua, T.; Zhang, S.; Chen, T. Soft Actor–Critic-Driven Adaptive Focusing under Obstacles. *Materials* **2023**, *16*, 1366. [PubMed]
107. An, S.; Zheng, B.; Shalaginov, M.Y.; Tang, H.; Li, H.; Zhou, L.; Dong, Y.; Haerinia, M.; Agarwal, A.M.; Rivero-Baleine, C.; et al. Deep Convolutional Neural Networks to Predict Mutual Coupling Effects in Metasurfaces. *Adv. Opt. Mater.* **2022**, *10*, 2102113. [CrossRef]
108. Ji, W.; Chang, J.; Xu, H.-X.; Gao, J.R.; Gröblacher, S.; Urbach, H.P.; Adam, A.J.L. Recent advances in metasurface design and quantum optics applications with machine learning, physics-informed neural networks, and topology optimization methods. *Light Sci. Appl.* **2023**, *12*, 169. [CrossRef] [PubMed]
109. Wu, B.; Wang, G.; Liu, K.; Hu, G.; Xu, H.-X. Equivalent-circuit-intervened deep learning metasurface. *Mater. Des.* **2022**, *218*, 110725. [CrossRef]
110. Zhang, F.; Wang, C.; Feng, W.; Liu, T.; Wang, Z.; Wang, Y.; Wang, M.; Xu, H.-X. Holographic communication using programmable coding metasurface. *Nanophotonics* **2024**, *13*, 1509–1519. [CrossRef] [PubMed]
111. Zhang, D.; Liu, Z.; Yang, X.; Xiao, J.J. Inverse Design of Multifunctional Metasurface Based on Multipole Decomposition and the Adjoint Method. *ACS Photonics* **2022**, *9*, 3899–3905. [CrossRef]
112. Wu, O.; Qian, C.; Fan, Z.; Zhu, X.; Chen, H. General Characterization of Intelligent Metasurfaces with Graph Coupling Network. *Laser Photonics Rev.* **2025**, *19*, 2400979. [CrossRef]
113. Jiang, J.; Fan, J.A. Global Optimization of Dielectric Metasurfaces Using a Physics-Driven Neural Network. *Nano Lett.* **2019**, *19*, 5366–5372. [CrossRef] [PubMed]
114. Ghorbani, F.; Beyraghi, S.; Shabanpour, J.; Oraizi, H.; Soleimani, H.; Soleimani, M. Deep neural network-based automatic metasurface design with a wide frequency range. *Sci. Rep.* **2021**, *11*, 7102. [CrossRef] [PubMed]
115. Asgari, S.; Fabritius, T. Multi-band terahertz anisotropic metamaterial absorber composed of graphene-based split square ring resonator array featuring two gaps and a connecting bar. *Sci. Rep.* **2024**, *14*, 7477. [CrossRef] [PubMed]
116. Ding, Z.; Su, W.; Luo, Y.; Ye, L.; Li, W.; Zhou, Y.; Zou, J.; Tang, B.; Yao, H. Metasurface inverse designed by deep learning for quasi-entire terahertz wave absorption. *Nanoscale* **2024**, *16*, 1384–1393. [CrossRef] [PubMed]
117. Kiani, M.; Zolfaghari, M.; Kiani, J. Transfer learning for inverse design of tunable graphene-based meta-surfaces. *J. Mater. Sci.* **2024**, *59*, 3516–3530. [CrossRef]
118. Li, E.; Wang, Y.; Jin, L.; Zong, Z.; Zhu, E.; Wang, B.; Wang, Q.; Yang, Z.; Yin, W.-Y.; Wei, Z. Current-diffusion model for metasurface structure discoveries with spatial-frequency dynamics. *Nat. Mach. Intell.* **2026**, *8*, 59–69. [CrossRef]
119. Sakoda, K. *Optical Properties of Photonic Crystals*, 2nd ed.; Springer: Berlin/Heidelberg, Germany, 2005.
120. Preble, S.; Lipson, M.; Lipson, H. Two-dimensional photonic crystals designed by evolutionary algorithms. *Appl. Phys. Lett.* **2005**, *86*, 061111. [CrossRef]
121. Tu, X.; Xie, W.; Chen, Z.; Ge, M.-F.; Huang, T.; Song, C.; Fu, H.Y. Analysis of Deep Neural Network Models for Inverse Design of Silicon Photonic Grating Coupler. *J. Light. Technol.* **2021**, *39*, 2790–2799. [CrossRef]
122. Jing, Y.; Teng, Q.; Luo, J.; Huang, C.; Sun, Z.; Lai, Y. Ultrabroadband transparent metamaterial absorbers designed by anomalous Brewster effect and gradient impedance matching optimized with deep neural network. *Phys. Rev. Appl.* **2025**, *23*, L051002. [CrossRef]
123. Ma, X.; Ma, Y.; Cunha, P.; Liu, Q.; Kudtarkar, K.; Xu, D.; Wang, J.; Chen, Y.; Wong, Z.J.; Liu, M.; et al. Strategical Deep Learning for Photonic Bound States in the Continuum. *Laser Photonics Rev.* **2022**, *16*, 2100658. [CrossRef]
124. Li, R.; Zhang, C.; Xie, W.; Gong, Y.; Ding, F.; Dai, H.; Chen, Z.; Yin, F.; Zhang, Z. Deep reinforcement learning empowers automated inverse design and optimization of photonic crystals for nanoscale laser cavities. *Nanophotonics* **2023**, *12*, 319–334. [CrossRef] [PubMed]
125. Li, Y.; Ao, Y.; Hu, X.; Lu, C.; Chan, C.T.; Gong, Q. Unsupervised Learning of non-Hermitian Photonic Bulk Topology. *Laser Photonics Rev.* **2023**, *17*, 2300481. [CrossRef]
126. Liu, Z.; Liu, X.; Xiao, Z.; Lu, C.; Wang, H.-Q.; Wu, Y.; Hu, X.; Liu, Y.-C.; Zhang, H.; Zhang, X. Integrated nanophotonic wavelength router based on an intelligent algorithm. *Optica* **2019**, *6*, 1367–1373. [CrossRef]
127. Song, T.; Jing, Y.; Shen, C.; Chu, H.; Luo, J.; Jia, R.; Wang, C.; Xiao, M.; Zhang, Z.-Q.; Peng, R.; et al. Nonlocality-enabled photonic analogies of parallel spaces, wormholes and multiple realities. *Nat. Commun.* **2025**, *16*, 8915. [CrossRef] [PubMed]

128. Unni, R.; Yao, K.; Zheng, Y. Deep Convolutional Mixture Density Network for Inverse Design of Layered Photonic Structures. *ACS Photonics* **2020**, *7*, 2703–2712. [CrossRef] [PubMed]
129. Unni, R.; Yao, K.; Han, X.; Zhou, M.; Zheng, Y. A mixture-density-based tandem optimization network for on-demand inverse design of thin-film high reflectors. *Nanophotonics* **2021**, *10*, 4057–4065. [CrossRef] [PubMed]
130. Ma, T.; Wang, H.; Guo, L.J. OptoGPT: A foundation model for inverse design in optical multilayer thin film structures. *Opto-Electron. Adv.* **2024**, *7*, 240062-1–240062-13. [CrossRef]
131. Zhang, D.; Bao, Q.; Chen, W.; Liu, Z.; Wei, G.; Xiao, J.J. Inverse design of an optical film filter by a recurrent neural adjoint method: An example for a solar simulator. *J. Opt. Soc. Am. B* **2021**, *38*, 1814–1821. [CrossRef]
132. Shao, G.; Zhou, T.; Yan, T.; Guo, Y.; Zhao, Y.; Huang, R.; Fang, L. Reliable, efficient, and scalable photonic inverse design empowered by physics-inspired deep learning. *Nanophotonics* **2025**, *14*, 2799–2810. [CrossRef] [PubMed]
133. Hooten, S.; Beausoleil, R.G.; Vaerenbergh, T.V. Inverse design of grating couplers using the policy gradient method from reinforcement learning. *Nanophotonics* **2021**, *10*, 3843–3856. [CrossRef]
134. Deng, R.; Liu, W.; Shi, L. Inverse design in photonic crystals. *Nanophotonics* **2024**, *13*, 1219–1237. [CrossRef] [PubMed]
135. Baba, T. Slow light in photonic crystals. *Nat. Photonics* **2008**, *2*, 465–473. [CrossRef]
136. Akahane, Y.; Asano, T.; Song, B.S.; Noda, S. High-Q photonic nanocavity in a two-dimensional photonic crystal. *Nature* **2003**, *425*, 944–947. [CrossRef] [PubMed]
137. Katsikas, G.; Peano, V.; Marquardt, F.; Verhagen, E. *Inverse Design of Two-Dimensional Photonic Crystals Through Physics-Informed Deep Learning*; SPIE: Bellingham, WA, USA, 2024; Volume PC12896.
138. Asano, T.; Noda, S. Optimization of photonic crystal nanocavities based on deep learning. *Opt. Express* **2018**, *26*, 32704–32717. [CrossRef] [PubMed]
139. Pavan, V.D.R.; Nikhil, V.; Dey, K.; Sharma, B.U.; Roy, S. Analysing group indices and dispersion characteristics of engineered photonic crystal waveguides using artificial neural network. *J. Opt.* **2024**, *53*, 1438–1446. [CrossRef]
140. Hirotani, K.; Shiratori, R.; Baba, T. Si photonic crystal slow-light waveguides optimized through informatics technology. *Opt. Lett.* **2021**, *46*, 4422–4425. [CrossRef] [PubMed]
141. Bole, M.; Ran, H.; Haotian, Y.; Huaqing, J.; Jianwei, C.; Kaida, T. Deep Learning-based Inverse Design of the Complete Photonic Band Gap in Two-Dimensional Photonic Crystals. *Curr. Nanosci.* **2023**, *19*, 423–431. [CrossRef]
142. Minkov, M.; Williamson, I.A.D.; Andreani, L.C.; Gerace, D.; Lou, B.; Song, A.Y.; Hughes, T.W.; Fan, S. Inverse Design of Photonic Crystals through Automatic Differentiation. *ACS Photonics* **2020**, *7*, 1729–1741. [CrossRef]
143. Luce, A.; Alaee, R.; Knorr, F.; Marquardt, F. Merging automatic differentiation and the adjoint method for photonic inverse design. *Mach. Learn. Sci. Technol.* **2024**, *5*, 025076. [CrossRef]
144. Cui, C.; Wei, G.; Saba, M.; Cao, Y.; Han, L. Deep Learning-Assisted Fourier Analysis for High-Efficiency Structural Design: A Case Study on Three-Dimensional Photonic Crystals Enumeration. *Small* **2026**, *22*, e11158. [CrossRef] [PubMed]
145. Asano, T.; Noda, S. Iterative optimization of photonic crystal nanocavity designs by using deep neural networks. *Nanophotonics* **2019**, *8*, 2243–2256. [CrossRef]
146. Liu, L.; Long, Y. Machine-learning-powered efficient design of photonic crystal cavities. *PhotoniX* **2025**, *6*, 37. [CrossRef]
147. Yan, H.; Hao, R.; Ye, B.; Jin, S. Exploring high-performance photonic crystal slow light waveguides through deep reinforcement learning. *Opt. Commun.* **2024**, *569*, 130830. [CrossRef]
148. Long, Y.; Ren, J.; Li, Y.; Chen, H. Inverse design of photonic topological state via machine learning. *Appl. Phys. Lett.* **2019**, *114*, 181105. [CrossRef]
149. Singh, R.; Agarwal, A.; W Anthony, B. Mapping the design space of photonic topological states via deep learning. *Opt. Express* **2020**, *28*, 27893–27902. [CrossRef] [PubMed]
150. Wang, B.-J.; Zhang, L.; Wang, B.-X.; Zhang, D.-P.; Xie, Y.-G.; Cai, J.-H. Inverse design of a valley-Hall photonic topological insulator based on tandem residual neural networks. *iScience* **2025**, *28*, 112276. [CrossRef] [PubMed]
151. Yu, Z.; Hao, R. Inverse design of bandgap for randomly encoded topological photonic crystals based on the SSH model via deep learning. *J. Opt. Soc. Am. B* **2025**, *42*, 1592–1600. [CrossRef]
152. Chen, Y.; Lan, Z.; Zhu, J. Inversely Designed Second-Order Photonic Topological Insulator With Multiband Corner States. *Phys. Rev. Appl.* **2022**, *17*, 054003. [CrossRef]
153. Tahersima, M.H.; Kojima, K.; Koike-Akino, T.; Jha, D.; Wang, B.; Lin, C.; Parsons, K. Deep Neural Network Inverse Design of Integrated Photonic Power Splitters. *Sci. Rep.* **2019**, *9*, 1368. [CrossRef] [PubMed]
154. Tang, Y.; Kojima, K.; Koike-Akino, T.; Wang, Y.; Wu, P.; Xie, Y.; Tahersima, M.H.; Jha, D.K.; Parsons, K.; Qi, M. Generative Deep Learning Model for Inverse Design of Integrated Nanophotonic Devices. *Laser Photonics Rev.* **2020**, *14*, 2000287. [CrossRef]
155. Ren, Y.; Zhang, L.; Wang, W.; Wang, X.; Lei, Y.; Xue, Y.; Sun, X.; Zhang, W. Genetic-algorithm-based deep neural networks for highly efficient photonic device design. *Photon. Res.* **2021**, *9*, B247–B252. [CrossRef]
156. Gostimirovic, D.; Grinberg, Y.; Xu, D.-X.; Liboiron-Ladouceur, O. Improving Fabrication Fidelity of Integrated Nanophotonic Devices Using Deep Learning. *ACS Photonics* **2023**, *10*, 1953–1961. [CrossRef]

157. Popoff, S.; Lerosey, G.; Fink, M.; Boccara, A.C.; Gigan, S. Image transmission through an opaque material. *Nat. Commun.* **2010**, *1*, 81. [CrossRef] [PubMed]
158. Li, S.; Deng, M.; Lee, J.; Sinha, A.; Barbastathis, G. Imaging through glass diffusers using densely connected convolutional networks. *Optica* **2018**, *5*, 803–813. [CrossRef]
159. Borhani, N.; Kakkava, E.; Moser, C.; Psaltis, D. Learning to see through multimode fibers. *Optica* **2018**, *5*, 960–966. [CrossRef]
160. Caramazza, P.; Moran, O.; Murray-Smith, R.; Faccio, D. Transmission of natural scene images through a multimode fibre. *Nat. Commun.* **2019**, *10*, 2029. [CrossRef] [PubMed]
161. Davoudi, N.; Deán-Ben, X.L.; Razansky, D. Deep learning optoacoustic tomography with sparse data. *Nat. Mach. Intell.* **2019**, *1*, 453–460. [CrossRef]
162. Liu, H.; Wang, F.; Jin, Y.; Ma, X.; Li, S.; Bian, Y.; Situ, G. Learning-based real-time imaging through dynamic scattering media. *Light Sci. Appl.* **2024**, *13*, 194. [CrossRef] [PubMed]
163. Jiang, R.; Smith, J.; Yi, Y.-T.; Sun, T.; Simonds, B.J.; Rollett, A.D. Deep learning approaches for instantaneous laser absorptance prediction in additive manufacturing. *npj Comput. Mater.* **2024**, *10*, 6. [CrossRef]
164. Vellekoop, I.M.; Mosk, A.P. Focusing coherent light through opaque strongly scattering media. *Opt. Lett.* **2007**, *32*, 2309–2311. [CrossRef] [PubMed]
165. Luo, J.; Li, X.; Zhang, X.; Guo, J.; Liu, W.; Lai, Y.; Zhan, Y.; Huang, M. Deep-learning-enabled inverse engineering of multi-wavelength invisibility-to-superscattering switching with phase-change materials. *Opt. Express* **2021**, *29*, 10527–10537. [CrossRef] [PubMed]
166. Jing, Y.; Chu, H.; Huang, B.; Luo, J.; Wang, W.; Lai, Y. A deep neural network for general scattering matrix. *Nanophotonics* **2023**, *12*, 2583–2591. [CrossRef] [PubMed]
167. Fan, P.; Zhao, T.; Su, L. Deep learning the high variability and randomness inside multimode fibers. *Opt. Express* **2019**, *27*, 20241–20258. [CrossRef] [PubMed]
168. Zhu, C.; Chan, E.A.; Wang, Y.; Peng, W.; Guo, R.; Zhang, B.; Soci, C.; Chong, Y. Image reconstruction through a multimode fiber with a simple neural network architecture. *Sci. Rep.* **2021**, *11*, 896. [CrossRef] [PubMed]
169. Barbastathis, G.; Ozcan, A.; Situ, G. On the use of deep learning for computational imaging. *Optica* **2019**, *6*, 921–943. [CrossRef]
170. Lyu, M.; Wang, H.; Li, G.; Zheng, S.; Situ, G. Learning-based lensless imaging through optically thick scattering media. *Adv. Photonics* **2019**, *1*, 036002. [CrossRef]
171. Lai, X.; Li, Q.; Chen, Z.; Shao, X.; Pu, J. Reconstructing images of two adjacent objects passing through scattering medium via deep learning. *Opt. Express* **2021**, *29*, 43280–43291. [CrossRef]
172. Li, J.; Zhang, Z.; Huang, M.; Xie, J.; Jia, F.; Liu, L.; Zhao, Y. Non-invasive imaging through scattering media with unaligned data using dual-cycle GANs. *Opt. Commun.* **2022**, *525*, 128832. [CrossRef]
173. Stern, G.; Katz, O. Noninvasive focusing through scattering layers using speckle correlations. *Opt. Lett.* **2019**, *44*, 143–146. [CrossRef] [PubMed]
174. Luo, Y.; Yan, S.; Li, H.; Lai, P.; Zheng, Y. Focusing light through scattering media by reinforced hybrid algorithms. *APL Photonics* **2020**, *5*, 016109. [CrossRef]
175. Turpin, A.; Vishniakou, I.; Seelig, J.d. Light scattering control in transmission and reflection with neural networks. *Opt. Express* **2018**, *26*, 30911–30929. [CrossRef] [PubMed]
176. Yang, J.; He, Q.; Liu, L.; Qu, Y.; Shao, R.; Song, B.; Zhao, Y. Anti-scattering light focusing by fast wavefront shaping based on multi-pixel encoded digital-micromirror device. *Light Sci. Appl.* **2021**, *10*, 149. [CrossRef] [PubMed]
177. Feng, B.Y.; Guo, H.; Xie, M.; Boominathan, V.; Sharma, M.K.; Veeraraghavan, A.; Metzler, C.A. NeuWS: Neural wavefront shaping for guidestar-free imaging through static and dynamic scattering media. *Sci. Adv.* **2023**, *9*, eadg4671. [CrossRef] [PubMed]
178. Liu, Y.; Ma, C.; Shen, Y.; Shi, J.; Wang, L.V. Focusing light inside dynamic scattering media with millisecond digital optical phase conjugation. *Optica* **2017**, *4*, 280–288. [CrossRef] [PubMed]
179. Shen, Y.; Liu, Y.; Ma, C.; Wang, L.V. Focusing light through scattering media by full-polarization digital optical phase conjugation. *Opt. Lett.* **2016**, *41*, 1130–1133. [CrossRef] [PubMed]
180. Cheng, Z.; Yang, J.; Wang, L.V. Intelligently optimized digital optical phase conjugation with particle swarm optimization. *Opt. Lett.* **2020**, *45*, 431–434. [CrossRef] [PubMed]
181. Shen, C.-Y.; Li, J.; Gan, T.; Li, Y.; Jarrahi, M.; Ozcan, A. All-optical phase conjugation using diffractive wavefront processing. *Nat. Commun.* **2024**, *15*, 4989. [CrossRef] [PubMed]
182. Matthès, M.W.; Bromberg, Y.; de Rosny, J.; Popoff, S.M. Learning and Avoiding Disorder in Multimode Fibers. *Phys. Rev. X* **2021**, *11*, 021060. [CrossRef]
183. Pan, T.; Ye, J.; Liu, H.; Zhang, F.; Xu, P.; Xu, O.; Xu, Y.; Qin, Y. Non-orthogonal optical multiplexing empowered by deep learning. *Nat. Commun.* **2024**, *15*, 1580. [CrossRef] [PubMed]
184. Sun, Y.; Shi, J.; Sun, L.; Fan, J.; Zeng, G. Image reconstruction through dynamic scattering media based on deep learning. *Opt. Express* **2019**, *27*, 16032–16046. [CrossRef] [PubMed]

185. Boniface, A.; Dong, J.; Gigan, S. Non-invasive focusing and imaging in scattering media with a fluorescence-based transmission matrix. *Nat. Commun.* **2020**, *11*, 6154. [CrossRef] [PubMed]
186. Kim, N.; Lee, D.; Yu, J.; Cho, S.W.; Lee, D.; Park, Y.; Hong, Y. Toward a robust and generalizable metamaterial foundation model. *npj Comput. Mater.* **2025**, *12*, 54. [CrossRef]
187. Marzban, R.; Adibi, A.; Pestourie, R. Inverse Design in Nanophotonics via Representation Learning. *Adv. Opt. Mater.* **2026**, *14*, e02062. [CrossRef]
188. Kim, M.; Park, H.; Shin, J. Nanophotonic device design based on large language models: Multilayer and metasurface examples. *Nanophotonics* **2025**, *14*, 1273–1282. [CrossRef] [PubMed]
189. Hu, S.; Li, M.; Xu, J.; Zhang, H.; Zhang, S.; Cui, T.J.; del Hougne, P.; Li, L. Electromagnetic metamaterial agent. *Light Sci. Appl.* **2025**, *14*, 12. [CrossRef] [PubMed]